REPORT No. 877

SUMMARY REPORT ON THE HIGH-SPEED CHARACTERISTICS OF SIX MODEL WINGS HAVING NACA 65_1-SERIES SECTIONS

By William T. Hamilton and Warren H. Nelson

SUMMARY

A summary of the results of wind-tunnel tests to determine the high-speed aerodynamic characteristics of six model wings having NACA 65_1-series sections is presented in this report. The 8-percent-thick wings were superior to the 10-percent and 12-percent-thick wings from the standpoint of power economy during level flight for Mach numbers above 0.76. However, airplanes that are to fly at Mach numbers below 0.76 will gain aerodynamically if the percentage thickness of the wing and the aspect ratio are both increased. The lift-curve slopes for the 8-percent-thick wings at 0.85 Mach number were roughly twice their low-speed values. The effectiveness of a 20-percent-chord flap on the 65_1-210 wing of aspect ratio 9 decreased rapidly as the Mach number was raised above 0.85 indicating probable difficulty in maintaining control by means of a 20-percent-chord flap on a wing or tail of this thickness at these Mach numbers. Dive-recovery flaps tested on the 8-percent-thick wing of aspect ratio 7.2 reached the maximum effectiveness at about 0.84 Mach number.

INTRODUCTION

The high-speed aerodynamic characteristics of six thin, finite-span wings having NACA 65_1-series airfoil sections are summarized and compared in this report. The high-speed characteristics were obtained from tests made in the Ames 16-foot high-speed wind tunnel. The tests were made to obtain data to aid in the design of airplanes having high level-flight speeds.

MODELS AND APPARATUS

The models were designed and constructed at the Ames Aeronautical Laboratory. The dimensions of the models are shown in figure 1, and the coordinates of the various wing sections are tabulated in table I. Figures 2 and 3 are photographs showing one of the model wings mounted in the Ames 16-foot high-speed wind tunnel. All the wings had NACA 65_1-series sections, 2.5 to 1 taper ratio, 3° dihedral, and a 10-foot span. The airfoil sections all had 0.2 ideal lift coefficient and a uniform chordwise load distribution (a=1) at this lift coefficient. The wing plan forms were such that the 25-percent-chord lines were unswept.

All of the wings except the 65_1-208 wing of aspect ratio 9 and 65_1-212 wing of aspect ratio 10.8 had steel spars with contoured Masonite coverings. The 65_1-208 wing of aspect ratio 9 was contoured from solid steel and the 65_1-212 wing of aspect ratio 10.8 had a steel spar with a contoured covering of "cerrobase" metal. The aft portion of the untwisted 65_1-210 wing of aspect ratio 9 was a 0.20-chord, aluminum, hinged flap with a radius nose.

A tail sting was attached to each wing for tests of the wing alone. A representative model bomber fuselage covered the sting during the tests of the wings having an aspect ratio 9 when the chordwise pressure distributions were measured. The fuselage was so placed that the wing incidence was 2° relative to the fuselage deck line.

The models were supported in the wind tunnel by four 5-percent-thick front struts and one 7-percent-thick rear strut.

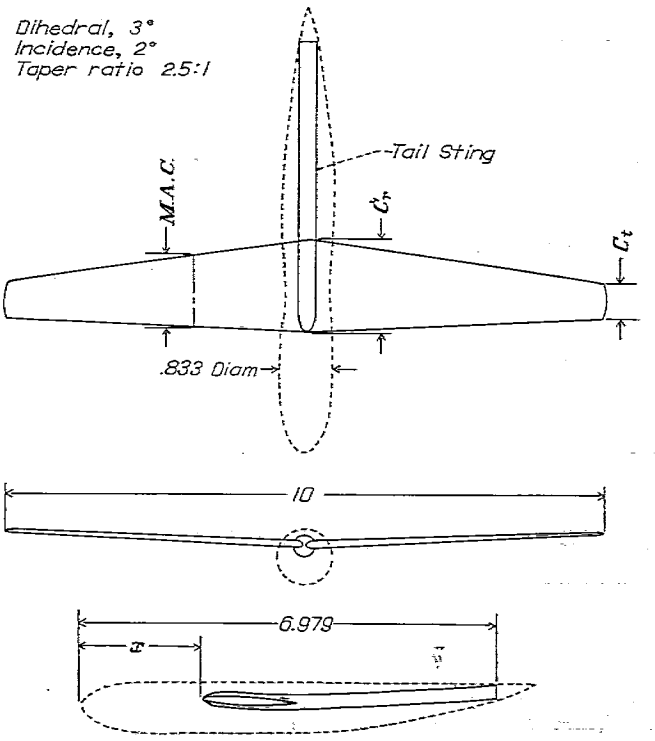

All dimensions in feet

Section	Aspect ratio	Area	C_r	C_t	MAC	x	Remarks
65_1-208	7.2	13.889	1.984	0.794	1.475	2.05	
65_1-208	9	11.111	1.587	.635	1.180	2.15	
65_1-210	9	11.111	1.587	.635	1.180	2.15	20% C flap.
65_1-210	9	11.111	1.587	.635	1.180	2.15	2° wash-out.
65_1-212	9	11.111	1.587	.635	1.180	2.15	
65_1-212	10.8	9.259	1.323	.529	.983	2.21	

FIGURE 1.—Dimensions of the six wings having NACA 65_1-series airfoil sections.

TABLE I.—ORDINATES OF THE THREE NACA 65_1-SERIES AIRFOIL SECTIONS

NACA 65_1-208 (a=1.0) Airfoil

Lower surface				Upper surface			
Sta.	Ord.	Sta.	Ord.	Sta.	Ord.	Sta.	Ord.
0	0	30.051	2.833	0	0	24.937	4.593
.553	.575	40.026	2.927	.447	.675	29.949	4.777
.809	.684	45.013	2.879	.691	.824	39.974	6.069
1.316	.836	50.000	2.754	1.184	1.050	44.987	5.069
2.574	1.079	59.978	2.266	2.426	1.451	50.000	4.960
5.082	1.428	69.966	1.581	4.918	2.060	60.022	4.408
7.585	1.692	79.964	.821	7.415	2.540	70.034	3.525
10.085	1.914	89.977	.147	9.915	2.948	80.036	2.413
15.081	2.257	94.988	−.064	14.919	3.603	90.023	1.181
20.073	2.515	100.000	0	19.927	4.107	95.012	.568
25.063	2.703	L. E. radius 0.434				100.000	0

NACA 65_1-210 (a=1.0) Airfoil

Lower surface				Upper surface			
Sta.	Ord.	Sta.	Ord.	Sta.	Ord.	Sta.	Ord.
0	0	40.032	3.925	0	0	29.936	5.732
.565	.719	50.000	3.709	.435	.819	39.968	6.067
.822	.859	59.973	3.075	.678	.999	50.000	5.915
1.331	1.059	64.964	2.652	1.169	1.237	60.027	5.217
2.592	1.385	69.957	2.184	2.408	1.757	65.036	4.712
5.102	1.859	79.956	1.191	4.898	2.491	70.043	4.128
7.606	2.221	84.962	.711	7.394	3.069	80.044	2.783
10.106	2.521	89.972	.293	9.894	3.555	85.038	2.057
15.101	2.992	94.986	−.010	14.890	4.338	90.028	1.327
20.091	3.346	100.000	0	19.902	4.938	95.014	.622
30.064	3.788	L. E. radius 0.687				100.000	0

NACA 65_1-212 (a=1.0) Airfoil

Lower surface				Upper surface			
Sta.	Ord.	Sta.	Ord.	Sta.	Ord.	Sta.	Ord.
0	0	50.000	4.654	0	0	39.961	7.068
.836	1.036	54.983	4.317	.664	1.176	50.000	6.860
1.346	1.277	59.963	3.872	1.154	1.491	55.017	6.507
2.609	1.686	64.957	3.351	2.391	2.058	60.032	6.014
5.122	2.287	69.950	2.771	4.878	2.919	65.043	5.411
7.627	2.745	79.948	1.548	7.373	3.593	70.050	4.715
10.217	3.128	84.955	.956	9.873	4.162	80.052	3.140
15.121	3.727	89.967	.429	14.879	5.073	85.045	2.302
20.110	4.178	94.983	.039	19.890	5.770	90.033	1.463
30.077	4.743	100.000	0	29.923	6.687	95.017	.671
40.039	4.926	L. E. radius 1.000				100.000	0

Ordinates in percent chord

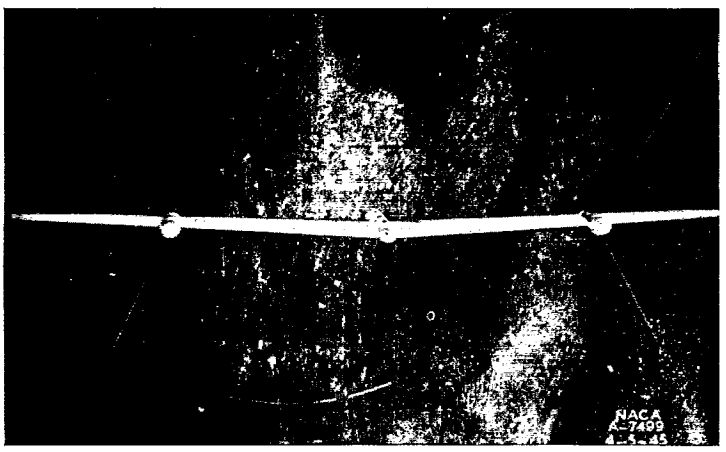

FIGURE 2.—Front view of the NACA 65_1-212 wing of aspect ratio 9, with tail sting, mounted in the Ames 16-foot high-speed wind tunnel.

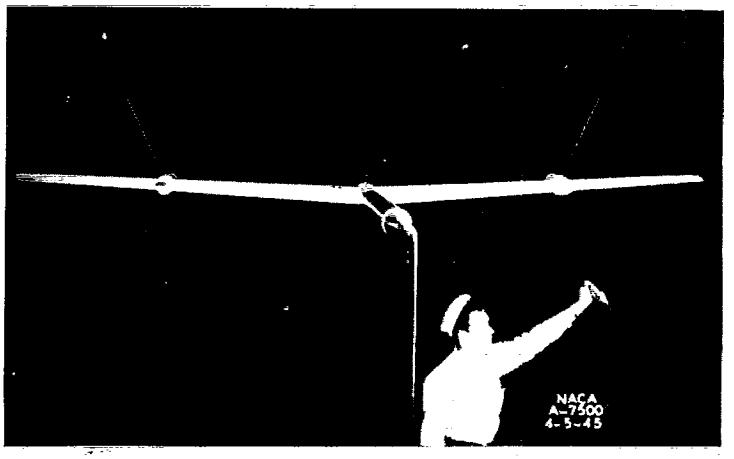

FIGURE 3.—Rear view of the NACA 65_1-212 wing of aspect ratio 9, with tail sting, mounted in the Ames 16-foot high-speed wind tunnel.

(See figs. 2 and 3.) Due to the limited thickness and strength of the model wings, it was necessary to attach the front support struts near the wing leading edges and to enclose the fittings in fairings. The angle of attack was changed through vertical movement of the rear support strut.

SYMBOLS

The following symbols are used in this report:

M	Mach number
a	mean-line designation, fraction of chord from leading edge over which design load is uniform
b	wing span, feet
S	wing area, square feet
A	aspect ratio (b^2/S)
$M.\ A.\ C.$	mean aerodynamic chord, feet
V	velocity, feet per second
ρ	mass density, slugs per cubic foot
q	dynamic pressure ($\frac{1}{2}\rho V^2$), pounds per square foot
α	angle of attack of wing reference plane, degrees
α_u	uncorrected angle of attack, degrees
α_{a_0}	angle of attack for zero lift, degrees
δ_f	wing flap deflection, degrees
C_L	lift coefficient (lift/qS)
C_D	drag coefficient (drag/qS)
C_{D_0}	profile drag coefficient $\left[C_D-\left(\frac{C_L^2}{\pi A}\right)\right]$
$C_{m_{c/4}}$	pitching-moment coefficient about quarter-chord point $\left[\frac{\text{pitching moment}}{qS(M.\ A.\ C.)}\right]$
a'	lift-curve slope ($dC_L/d\alpha$)
a'_0	section lift-curve slope $\left(\frac{a'\pi A}{\pi A-a'}\right)$
p	local static pressure, pounds per square foot
p_0	free-stream static pressure, pounds per square foot
P	pressure coefficient $[(p-p_0)/q]$
P_{min}	minimum pressure coefficient
P_{cr}	pressure coefficient corresponding to the local speed of sound
L/D	ratio of lift to drag
W	airplane weight, pounds
HP	horsepower

REDUCTION OF DATA

The Mach number and dynamic-pressure calibrations were evaluated from surveys of the test-section static pressure made with multiple static-pressure booms while the struts were mounted in the tunnel. These calibrations were made and constriction corrections, due to the presence of the model, were applied in the manner described in reference 1. The maximum variation of the airspeed from the mean value at 0.80 Mach number was 2.5 percent at a position 4 percent of the wing span away from the strut tip fairings, and 1 percent at a position 12.5 percent of the wing span away. The constriction correction due to the presence of the model amounted to about a 0.7-percent increase in Mach number at 0.80 Mach number and a 1.4-percent increase at 0.85 Mach number. The calibration is believed to be accurate to within 0.01 Mach number, but the data above a Mach number of 0.88 are shown dotted because their validity is uncertain due to the proximity of the tunnel-choking Mach number. The average inclination of the tunnel air flow was determined from the results of tests with a model wing first upright, then inverted.

The tare forces of the front struts were obtained from a series of tests during which the model was supported first upright, then inverted, on the four front struts and the lower rear strut, and then upright and inverted on the upper front struts and the lower rear strut. Since the structural limitations of the front struts require that only tension loads be imposed, their tare forces could not be evaluated over the complete angle-of-attack range. As a result, the tare forces were extrapolated in part. During the tests for determining these tares, the models were restrained laterally by streamlined tie rods attached to their wing tips. Since the front strut tares varied with the critical speed of the model wing being tested, it was necessary to determine these tares for each model wing.

The tare forces of the rear support strut were determined from tests of one of the models, supported by an auxiliary rear strut mounted from above, first with the lower rear strut in place and then with it removed.

Difficulty was encountered in keeping the model support-strut surfaces uniformly smooth; for this reason the tare forces of the struts did not remain always constant. Even relatively small variations in the tare forces were serious because the exposed strut area in the tunnel was over three times the model wing area. These variations in the drag of the support struts are believed to be partly responsible for the different minimum drag coefficients measured for the different wings at the lower Mach numbers.

The effect of the strut tip fairings on the measured forces was evaluated from tests with and without dummy fairings mounted midway between the model center line and the point of strut attachment on the model wing. A study of the air flow, as shown by the tufts glued to the surface of the model wings, indicated that the wings stalled first just inboard of the strut tip fairings. This premature stall probably affected the stall of other portions of the model wings and the maximum lift of the wings. The effect of the tail sting was approximated from model tests with and without a pair of dummy tail stings mounted on the wing between the center line and the strut tip fairings.

The data were corrected for tunnel-wall effects according to the methods of reference 2 by the addition of the following:

$$\Delta\alpha \text{ (deg)} = 0.0372\, SC_L$$
$$\Delta C_D = 0.006495\, SC_L^2$$

The pitching moments were referred to the 25-percent point of the mean aerodynamic chord for each wing.

DISCUSSION

The variation of test Reynolds number with Mach number for the various model wings is presented in figure 4.

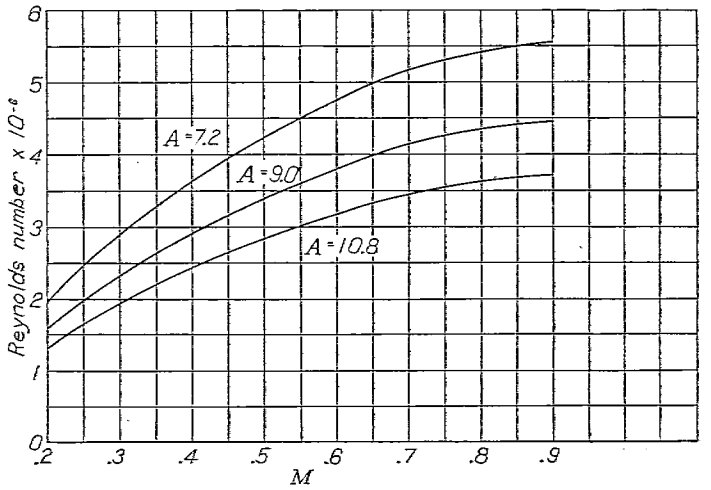

FIGURE 4.—Variation of test Reynolds number with Mach number for the model wings of three different aspect ratios.

The Reynolds numbers ranged from 1,300,000 to 2,000,000 at 0.20 Mach number and from 3,700,000 to 5,500,000 at 0.90 Mach number.

The aerodynamic characteristics of the six model wings are presented in figures 5 to 22. Figure 23 is a comparison of lift-curve slopes for the various wings and figure 24 is a comparison of the same data corrected to infinite aspect ratio by use of the simple Prandtl theory. The lift-curve slopes increased with Mach number less rapidly than predicted by Glauert's relation for two-dimensional flow $(1/\sqrt{1-M^2})$ for Mach numbers below 0.50 and more rapidly for Mach numbers above 0.50 and below that of lift divergence. The variation of the lift-curve slopes at the low Mach numbers for the different wings is believed at least partly due to the test Reynolds numbers in this region. The wing with NACA 65$_1$–212 airfoil sections and a 10.8 aspect ratio had the greatest lift-curve slope at the lower Mach numbers. At 0.20 Mach number this wing was operating at Reynolds numbers of 1,860,000 and 740,000 at the root and tip, respectively. Figure 38 of reference 3 indicates a general tendency toward a greater lift-curve slope as the Reynolds number is decreased. As the Mach number was increased, the slopes of the lift curves ceased to increase for Mach numbers above about 0.78 for the 12-percent-thick wings, 0.81 Mach number for the 10-percent-thick wings, and 0.85 Mach number for the 8-percent-thick wings. When the Mach number was increased above that at which the

lift-curve slope ceased to increase, the lift-curve slope decreased rapidly, and for the 12-percent-thick wings was only about 30 percent of the low-speed value at 0.875 Mach number. It should be noted that for the 8-percent-thick wings the lift-curve slope approximately doubled as the Mach number was increased from 0.20 to 0.85. This factor must be considered in the longitudinal-stability calculations for airplanes that are to incorporate this type of wing and fly over this range of Mach numbers. The slope of the lift curve for the 65_1–210 wing was essentially the same with and without 2° washout.

Figure 25 shows the changes in the angle of attack for zero lift that occurred for the wings as the Mach number was increased from 0.20 to 0.90. In general, the angle of attack for zero lift remained unchanged as the Mach number was increased from 0.20 to 0.65, and then increased slightly up to 0.75 Mach number for the 8-percent-thick wings and up to 0.70 Mach number for the 12-percent-thick wings. A further increase in the Mach number caused the angle of attack for zero lift to decrease slightly until 0.88 Mach number was reached for the 8-percent-thick wings and 0.84 Mach number for 12-percent-thick wings. A decrease in the angle of attack for zero lift will add a climbing moment to a conventional airplane with a fixed horizontal stabilizing surface and an increase will add a diving moment, other factors being unchanged.

A comparison of lift-curve slope ($dC_L/d\alpha$) with flap effectiveness ($dC_L/d\delta_f$) for the 10-percent-thick wing at lift coefficients near zero is presented in figure 26 and shows that the two varied in roughly the same manner up to about 0.82 Mach number, a flap deflection being about half as effective as the same change in angle of attack. As the Mach number was increased above 0.82, both the lift-curve slope and flap effectiveness decreased rapidly so that a flap deflection was only about one-third as effective as the same change in angle of attack at 0.875 Mach number and about one-sixth as effective at 0.90 Mach number. This large loss in flap effectiveness indicates probable difficulty in obtaining control by means of flapped surfaces at subsonic Mach numbers above those of lift divergence.

Figure 27 is a presentation of the increments of pitching-moment coefficient and angle of attack for a given lift coefficient resulting from a 30° deflection of a pair of dive-recovery flaps located at the 30-percent-chord point on the 65_1–208 wing of aspect ratio 7.2. The angle of attack for zero lift was increased slightly at the low Mach numbers by deflection of the dive-recovery flaps, was unchanged at 0.65 Mach number, and was decreased 1.5° at 0.90 Mach number. As previously pointed out, a decrease in the angle of attack for zero lift of a conventional airplane causes a climbing moment because of the action of the fixed horizontal tail. The change in pitching-moment coefficient of the wing resulting from deflection of the dive-recovery flaps at zero lift coefficient is about 0.025 at 0.20 Mach number, 0.040 at 0.80 Mach number, and 0.0 at 0.87 Mach number. For a conventional airplane with this wing-dive-recovery-flap combination, the dive-recovery-flap effectiveness would be a maximum at about 0.84 Mach number (considering the changes in both wing pitching-moment coefficient and angle of attack for zero lift) if the horizontal tail had a critical speed above that of the wing. In view of previous dive-recovery-flap experiments, this result indicates that these flaps reach their maximum effectiveness at a Mach number near that of lift divergence, which is dependent on the wing critical Mach number.

The drag coefficients of the five untwisted wings are compared for three lift coefficients in figure 28 and the profile-drag coefficients are compared for three Mach numbers in figure 29. The Mach number of drag divergence at zero lift coefficient was 0.78 for the 12-percent-thick wings, 0.81 for the 10-percent-thick wings, and 0.84 for the 8-percent-thick wings. The variation in profile-drag coefficient at the lower Mach numbers and lift coefficients is believed partially due to variations in the drag of the model-support struts for which corrections could not be made, as stated in the discussion of the tares.

Figure 30 shows the variations of the minimum measured pressure coefficient at a wing station 10 inches from the center line for the wings of three different thicknesses and aspect ratio 9. The unusual variation for the 65_1–208 wing between 0.20 and 0.50 Mach number was due to a small minimum-pressure peak that formed near the nose on this wing at the low speeds and moderate angles of attack. The fact that this peak disappeared at the higher Mach numbers indicates the possibility that it may be due only to the low Reynolds numbers of the low Mach number tests. The critical Mach numbers of the three wings at 0° angle of attack and this wing station were 0.74, 0.77, and 0.79 for the 12-,10-, and 8-percent-thick wings, respectively. The peak-negative-pressure coefficients continued to increase until the critical Mach number had been exceeded by about 0.08 and then decreased.

Figures 31, 32, and 33 compare the lift-drag ratios for level flight of three wings, all having the same absolute span and thickness but different chords. The lift-drag ratios were determined on a constant-weight basis from an assumed wing loading for the aspect-ratio-9 wing. The equation for the power required to maintain level flight can be put in the following form:

$$HP_{required} = (D/L)\ (WV/375)$$

Since the power required varies inversely as (L/D), figure 31 shows that at sea level the thicker, higher-aspect-ratio wing requires less power for Mach numbers below about 0.77. From about 0.77 Mach number to 0.82, the 10-percent-thick wing is superior; and, for Mach numbers above about 0.82, the low-aspect-ratio, thinner wing has less drag. An increase in the wing loading from 40 pounds to 80 pounds per square foot has essentially no effect on the range of Mach numbers over which each wing was superior in power economy at sea level. However, the power economy with each wing may be increased by increasing the wing loading, and at 0.70 Mach number and sea level an increase in the wingloading from 40 pounds to 80 pounds per square foot would double the airplane weight carried, and for the thicker, higher-aspect-ratio wing would increase the power required by the wing by only about 18 percent. Similar comparisons at 40,000 feet altitude in figure 33 show the 8-percent thick,

7.2-aspect-ratio wing to have less drag than the other two at Mach numbers above about 0.78 for wing loading of 40 to 60 pounds per square foot, and above 0.76 for an 80-pound-per-square-foot wing loading. An increase in the wing loading at 40,000 feet altitude did not reduce the drag per pound carried as much as at sea level. An airplane, flying at 0.75 Mach number with the 10-percent-thick aspect-ratio-9 wing, could increase its load 50 percent at an increase of 41 percent in the power required by the wing by changing from a 40- to a 60-pound-per-square-foot wing loading. An increase in the wing loading to 80 pounds per square foot would require an increase of 114 percent in the power required by the wing over that with a 40-pound wing loading. Therefore, the power per pound carried would be higher with the 80-pound wing loading than with the 40-pound wing loading.

Figures 34, 35, and 36 present comparisons of lift-drag ratios for three wings having the same plan form but different thicknesses. At sea level, the 8-percent-thick wing required less power for flight Mach numbers above about 0.75 for wing loadings from 40 to 80 pounds; and the 12-percent-thick wing was superior below this Mach number. As in previous comparisons at sea level, increasing the wing loading from 40 to 80 pounds per square foot reduced the power required by the wing per pound carried. The comparisons for flight at 40,000 feet (fig. 36) show the 12-percent-thick wing to be the more economical of power for Mach numbers below 0.75, and the 8-percent-thick wing to have less drag for Mach numbers above 0.75.

These comparisons show that the choice of a wing section, plan form, and loading for a high-speed airplane should be dictated by the speed and altitude at which the proposed airplane is to fly in order to obtain the most efficient wing characteristics.

Figures 37 and 38 are comparisons of the wing pitching-moment coefficients at lift coefficients for level flight of the three wings having the same absolute span and thickness but different chords. All three wings had about the same pitching-moment coefficients for level flight at a given loading, altitude, and Mach number for Mach numbers below about 0.84. The pitching-moment coefficients of the wing for level flight, in general, decreased slightly as the Mach number was increased. The level-flight pitching-moment coefficients for the 12-percent-thick, 10.8-aspect-ratio wing began increasing with Mach number as the Mach number exceeded 0.82. This increase in the pitching-moment coefficients of the wing at high Mach numbers is particularly desirable from the standpoint of recovery from high Mach number dives. Figures 39 and 40 show similar comparisons of the pitching-moment coefficients for the three wings varying only in thickness and show a close resemblance to the comparisons of figures 37 and 38, indicating that the major changes in pitching-moment coefficient at the high Mach numbers are due mainly to the wing section.

Figures 41 and 42 present the angles of attack of the various wings necessary to maintain the lift coefficients required for level flight. The angles of attack generally decreased as the Mach number was increased, as would be expected if no change in the angle of attack for zero lift or in the lift-curve slope were encountered. At the highest Mach numbers, and expecially at higher altitudes, the 8-percent-thick wings show no tendency to require an increase in the angle of attack for level flight with Mach number as do the thicker wings. This continued decrease in the necessary angle of attack is particularly desirable from the standpoint of control in high Mach numbers dives where an increase in the necessary wing angle of attack will cause an increase of the tail angle of attack, for a conventional airplane, and thereby a diving moment for the airplane. This diving moment may become so severe that a pilot could not exert the control necessary to maintain a level-flight attitude.

CONCLUSIONS

The lift-curve slopes of the model wings increased with Mach number less rapidly than predicted by Glauert's factor for two-dimensional-flow $(1/\sqrt{1-M^2})$ for Mach numbers between 0.20 and 0.50 and more rapidly for Mach numbers above 0.50 but below that of lift divergence. The lift-curve slopes ceased to increase with Mach number above about 0.78 for the 12-percent-thick wings, 0.81 for the 10-percent-thick wings, and 0.85 for the 8-percent-thick wings. The lift-curve slopes of the 8-percent-thick wings were roughly twice their low-speed values at 0.85 Mach number.

The effectiveness of a 20-percent-chord flap on the 65_1–210 wing of aspect ratio 9 decreased rapidly as the Mach number was increased beyond that of lift divergence for the wing. Difficulty will probably be encountered in maintaining control of an airplane solely by means of trailing-edge flaps at subsonic Mach numbers above 0.87, especially if the surfaces have a thickness of 10 percent or greater.

Dive recovery flaps on the 8-percent-thick wing of aspect ratio 7.2 reached their maximum effectiveness at about 0.84 Mach number. In view of previous dive-recovery-flap tests, this result indicates that the Mach number at which this flap effectiveness is a maximum is related to the critical Mach number of the wing to which the flaps are attached.

Of the six wings tested, the one having 12-percent-thick sections and an aspect ratio of 10.8 would give the most efficient operation for airplanes that are to fly near sea level and at Mach numbers below 0.77. The 8-percent-thick wing had less drag than the thicker wings of the same plan form for Mach numbers above about 0.76.

AMES AERONAUTICAL LABORATORY,
NATIONAL ADVISORY COMMITTEE FOR AERONAUTICS,
MOFFETT FIELD, CALIF. *October 19, 1945.*

REFERENCES

1. Nissen, James M., Gadeberg, Burnett L., and Hamilton, William T.: Correlation of the Drag Characteristics of a P–51B Airplane Obtained From High-Speed Wind-Tunnel and Flight Tests. NACA ACR No. 4K02, 1945.
2. Silverstein, Abe, and White, James A.: Wind-Tunnel Interference With Particular Reference to Off-Center Positions of the Wing and to the Downwash at the Tail. NACA Rep. No. 547, 1935.
3. Jacobs, Eastman N., and Sherman, Albert: Airfoil Section Characteristics as Affected by Variations of the Reynolds Number. NACA Rep. No. 586, 1937.

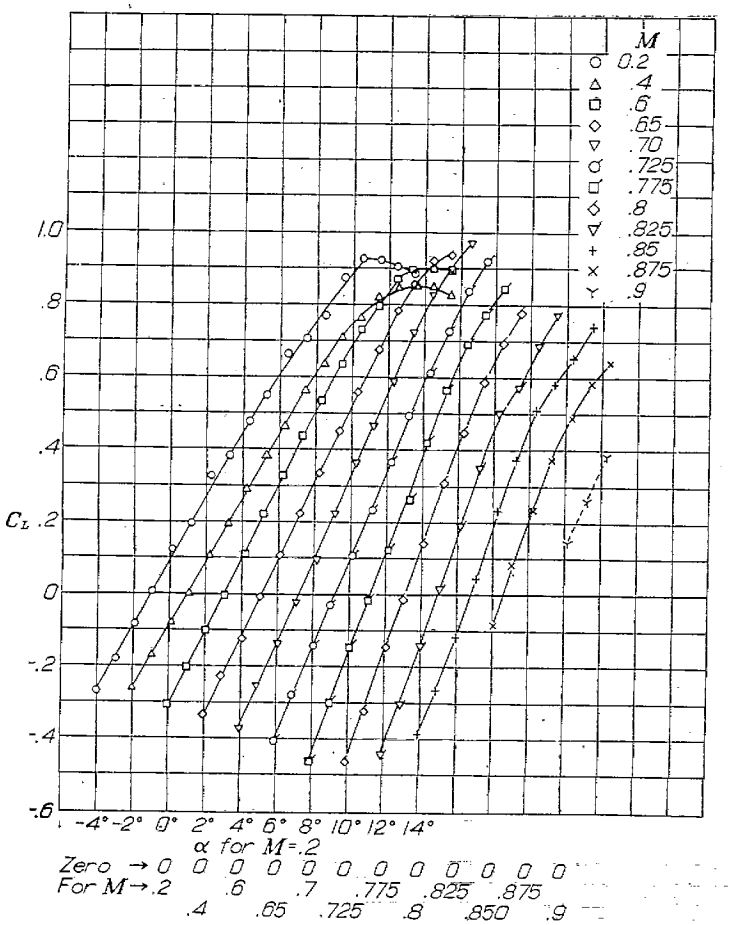

FIGURE 5.—Variation of lift coefficient with angle of attack for the NACA 65₁-208 wing of aspect ration 7.2.

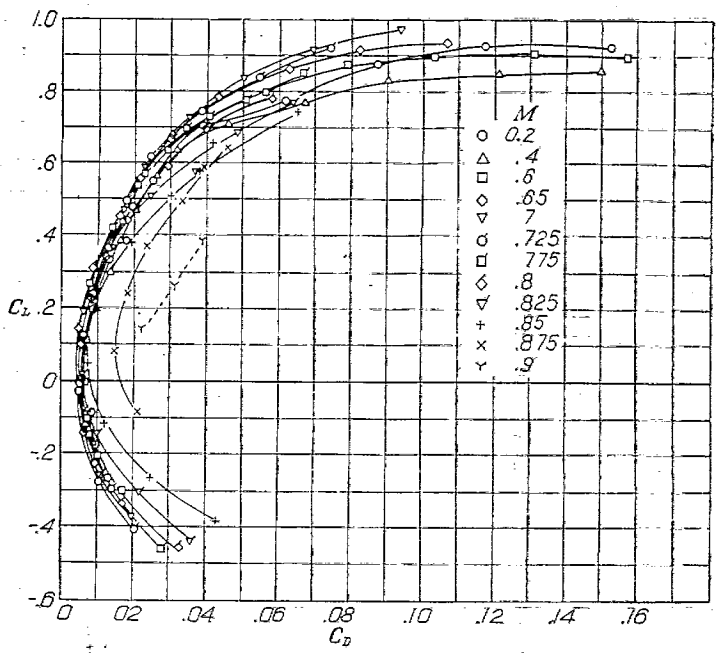

FIGURE 6.—Variation of drag coefficient with lift coefficient for the NACA 65₁-208 wing of aspect ratio 7.2.

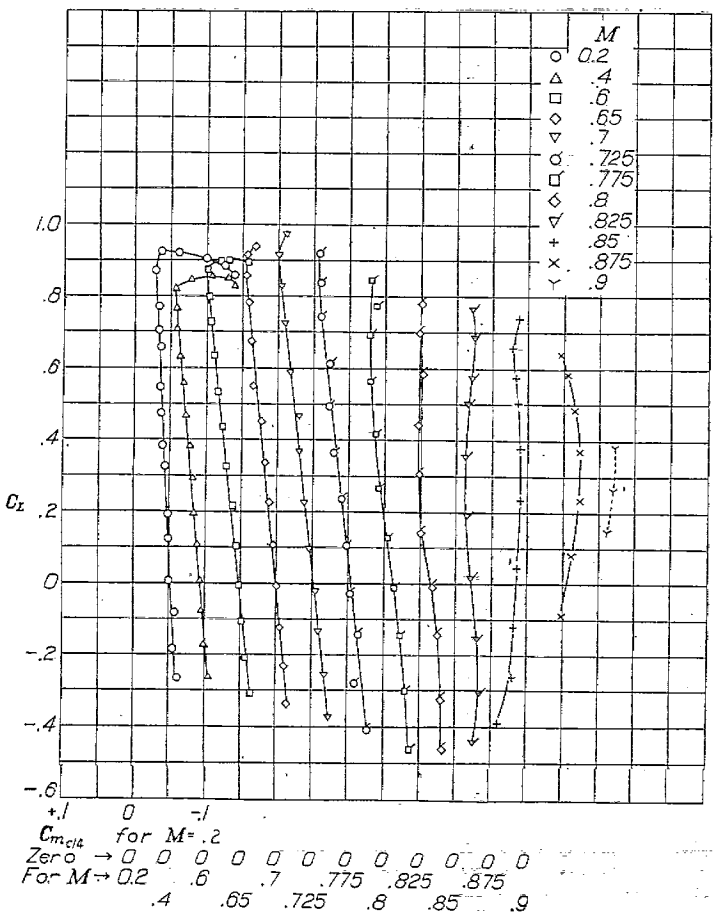

FIGURE 7.—Variation of pitching-moment coefficient with lift coefficient for the NACA 65₁-208 wing of aspect ratio 7.2.

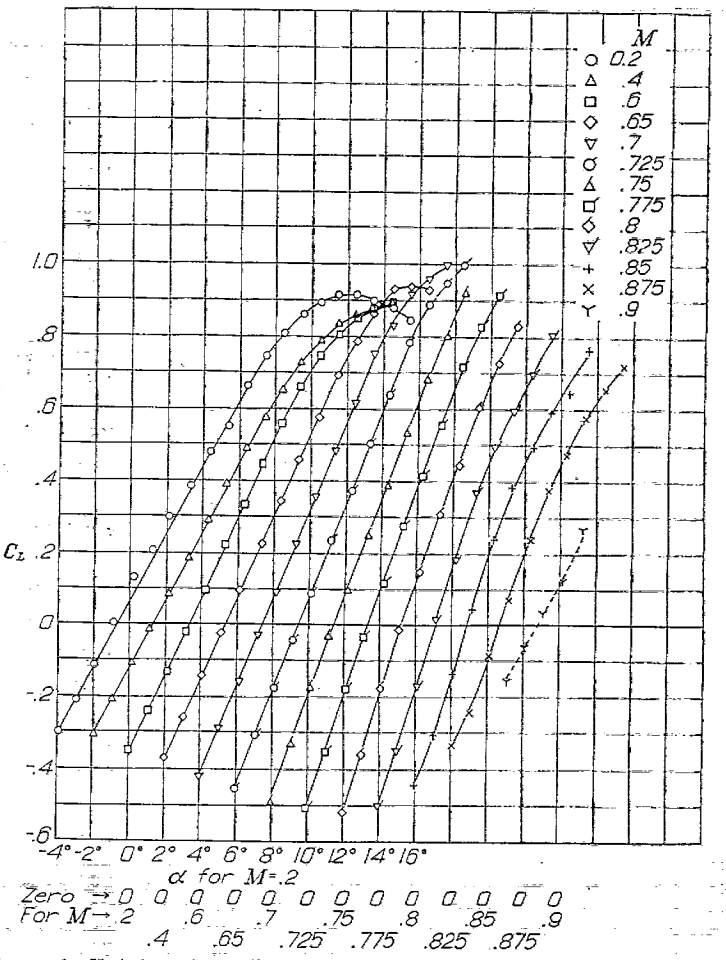

FIGURE 8.—Variation of lift coefficient with angle of attack for the NACA 65₁-208 wing of aspect ratio 9.

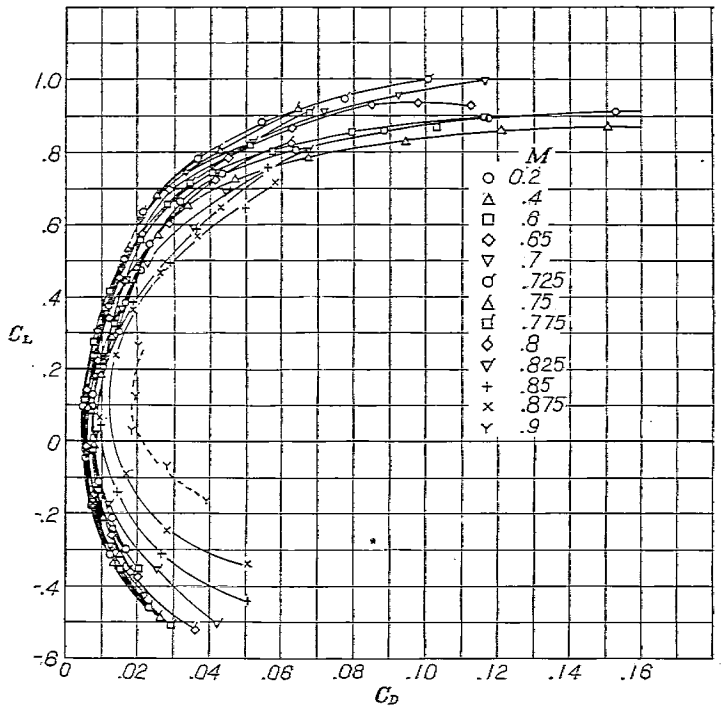

FIGURE 9.—Variation of drag coefficient with lift coefficient for the NACA 65$_1$-208 wing of aspect ratio 9.

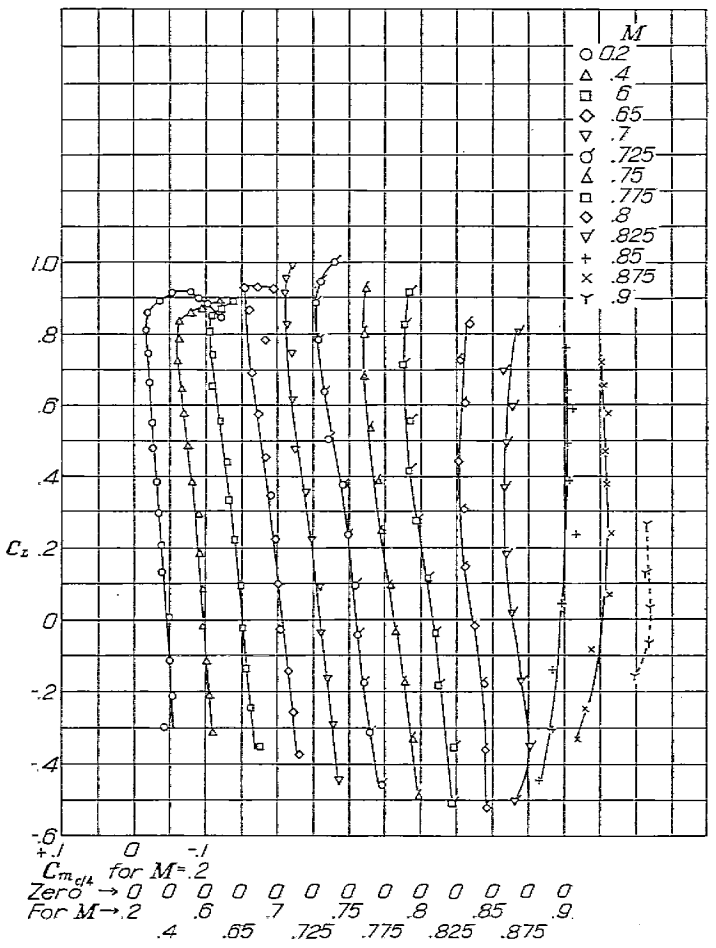

FIGURE 10.—Variation of pitching-moment coefficient with lift coefficient for the NACA 65$_1$-208 wing of aspect ratio 9.

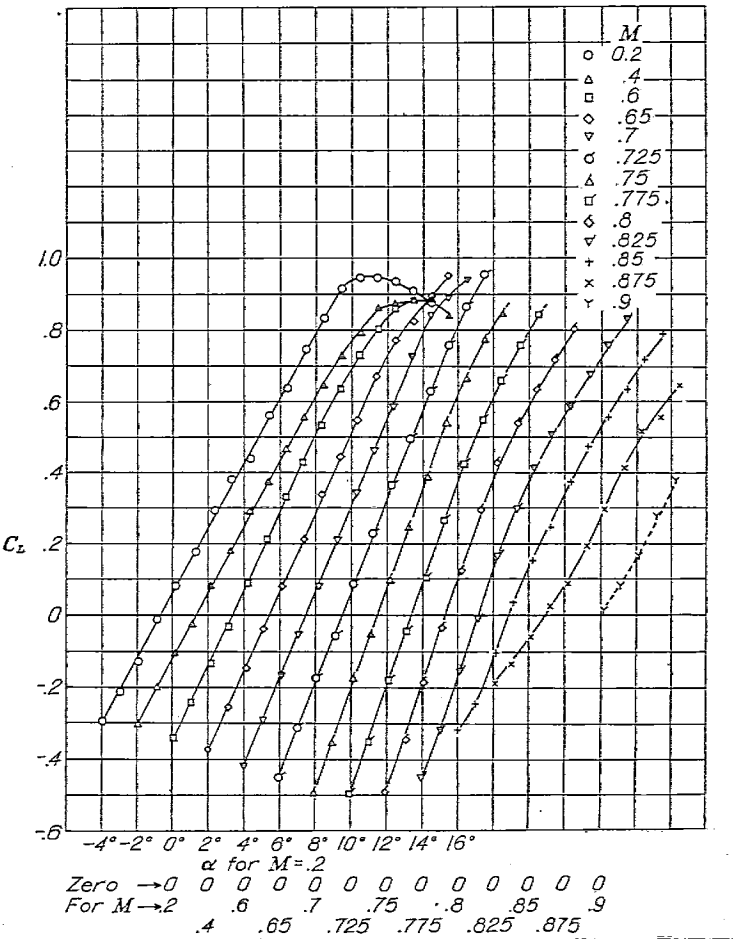

FIGURE 11.—Variation of lift coefficient with angle of attack for the NACA 65$_1$-210 wing of aspect ratio 9. δ_f, 0°.

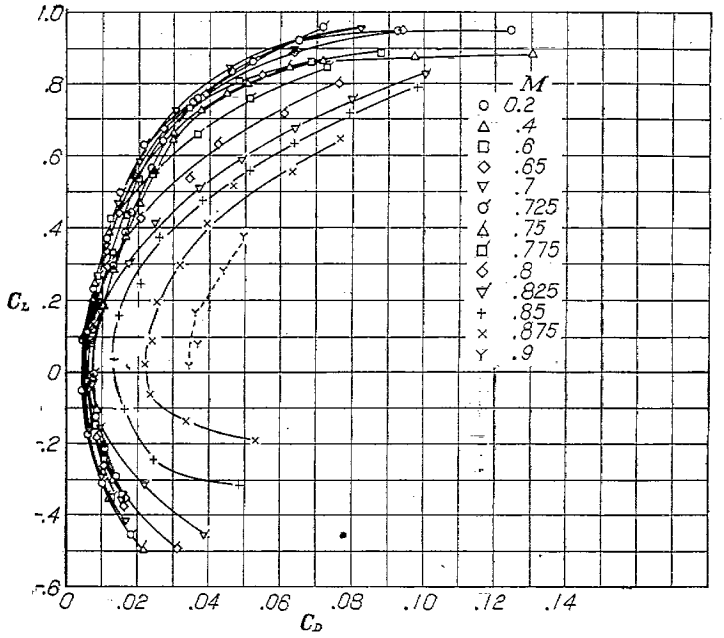

FIGURE 12.—Variation of drag coefficient with lift coefficient for the NACA 65$_1$-210 wing of aspect ratio 9. δ_f, 0°.

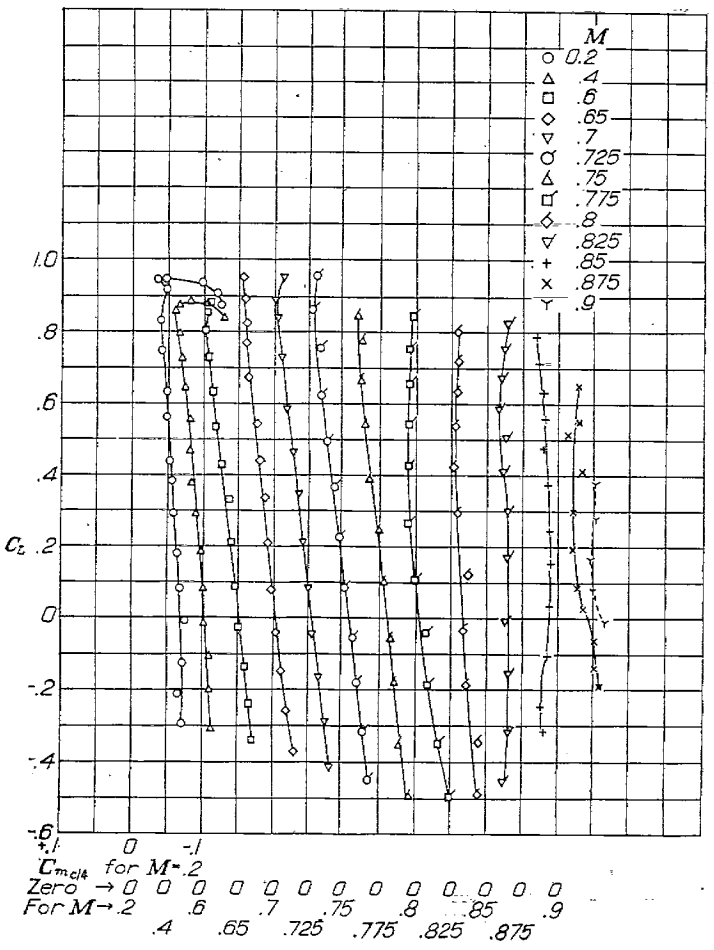

FIGURE 13.—Variation of pitching moment coefficient with lift coefficient for the NACA 65$_1$-210 wing of aspect ratio 9. δ_f, 0°.

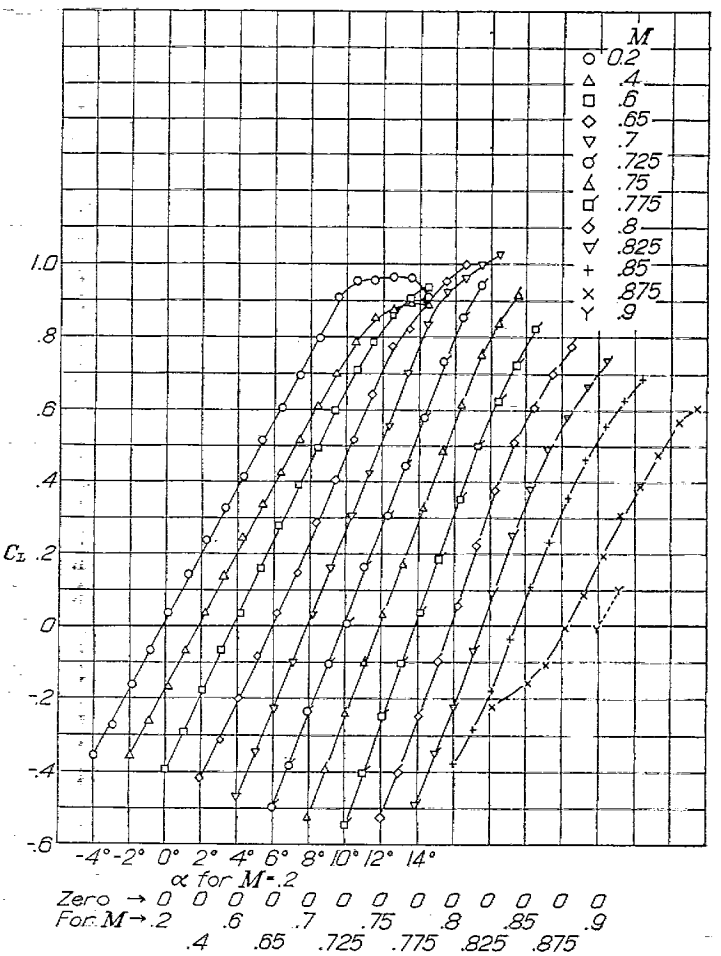

FIGURE 14.—Variation of lift coefficient with angle of attack for the NACA 65$_1$-210 wing with 2° twist and an aspect ratio of 9.

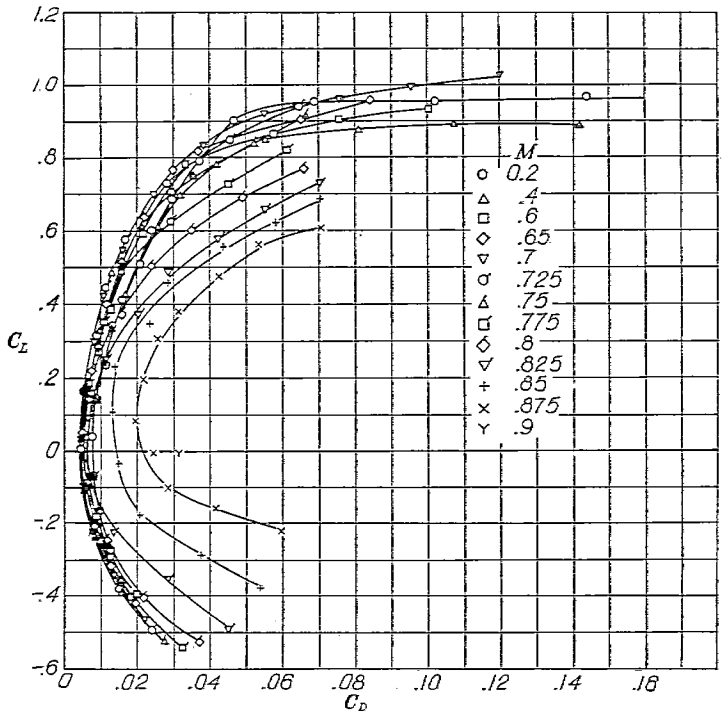

FIGURE 15.—Variation of drag coefficient with lift coefficient for the NACA 65$_1$–210 wing with 2° twist and an aspect ratio of 9.

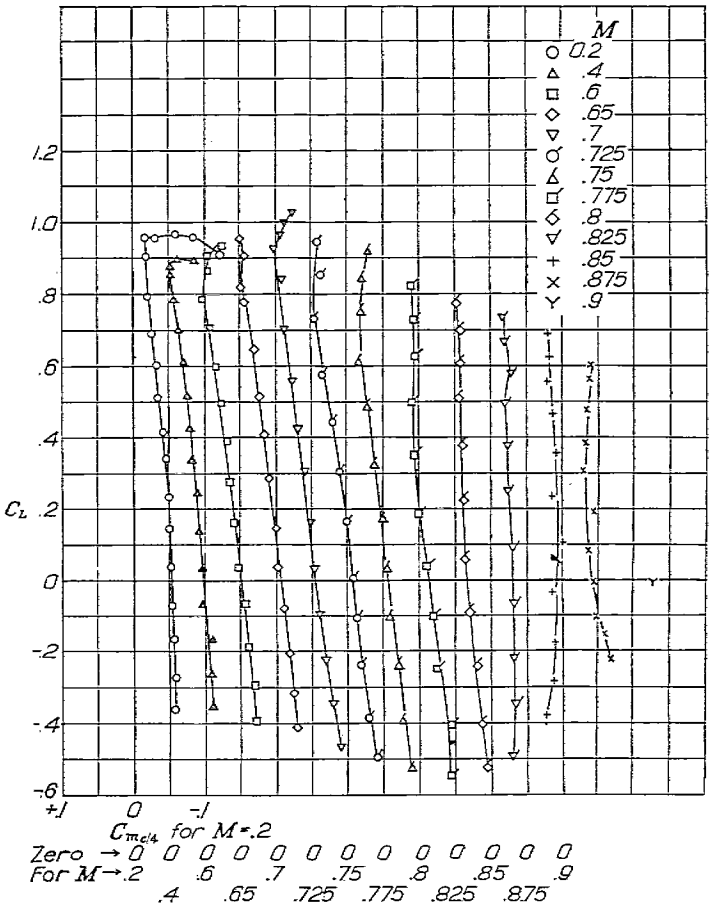

FIGURE 16.—Variation of pitching-moment coefficient with lift coefficient for the NACA 65$_1$–210 wing with 2° twist and an aspect ration of 9.

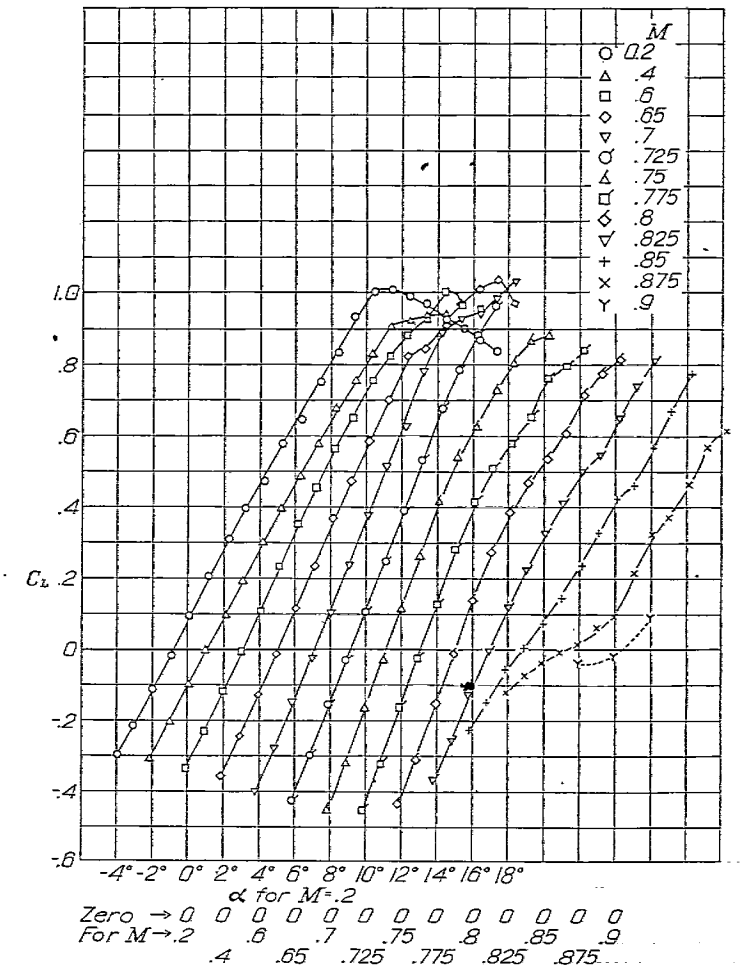

FIGURE 17.—Variation of lift coefficient with angle of attack for the NACA 65$_1$–212 wing of aspect ratio 9.

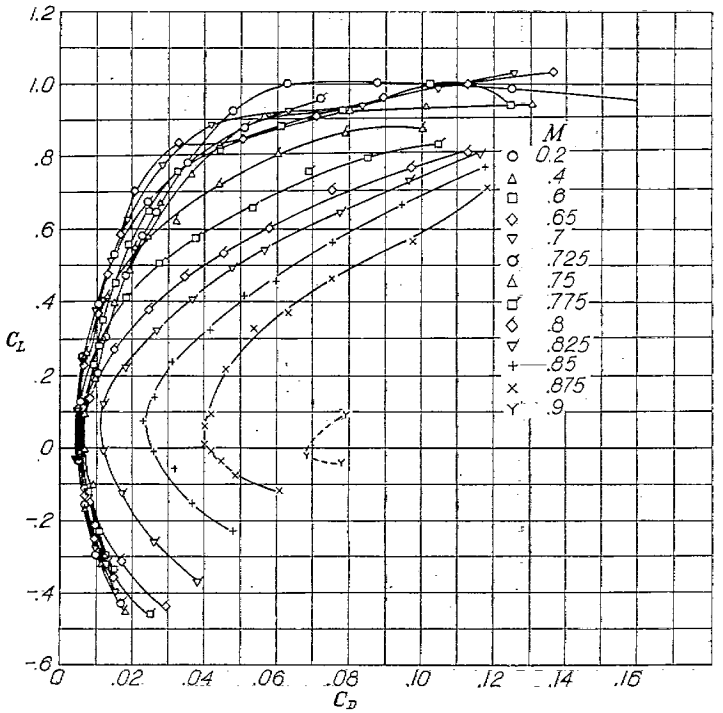

FIGURE 18.—Variation of drag coefficient with lift coefficient for the NACA 65$_1$-212 wing of aspect ratio 9.

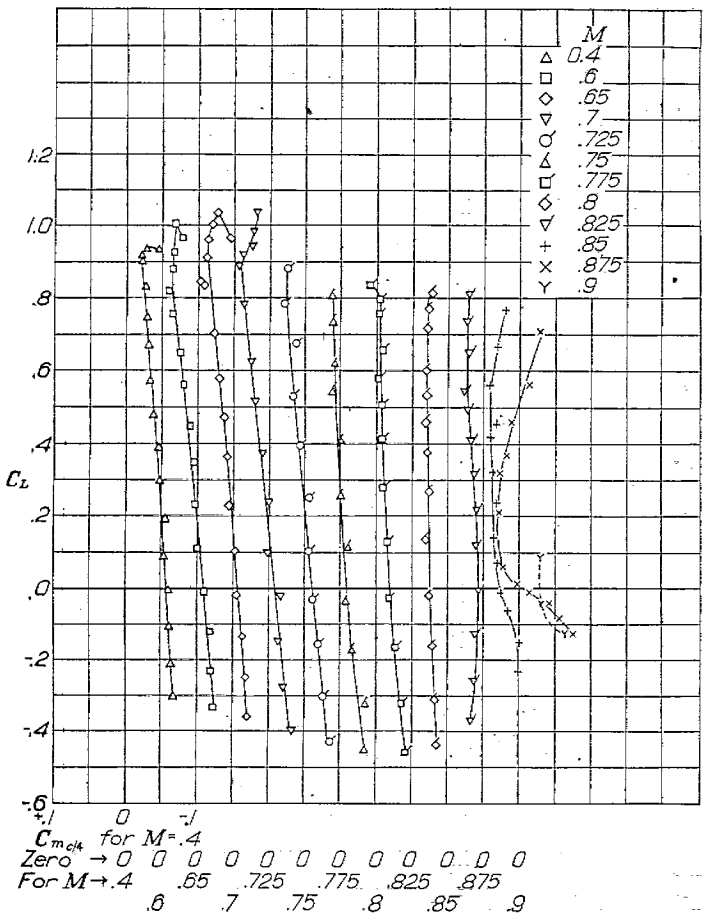

FIGURE 19.—Variation of pitching-moment coefficient with lift coefficient for the NACA 65$_1$-212 wing of aspect ratio 9.

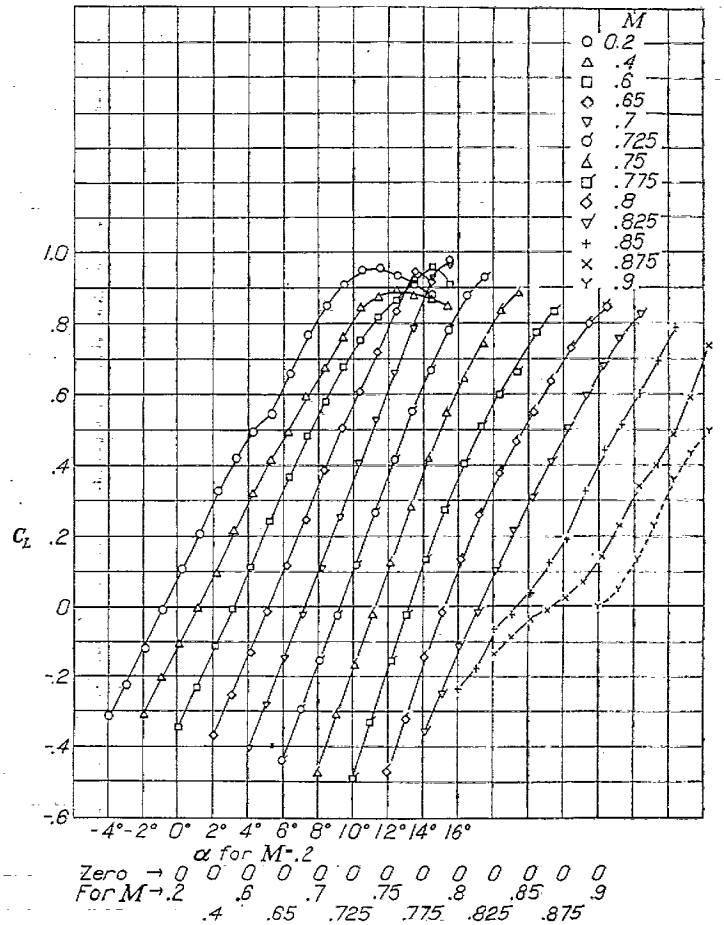

FIGURE 20.—Variation of lift coefficient with angle of attack for the NACA 65$_1$-212 wing of aspect ratio 10.8.

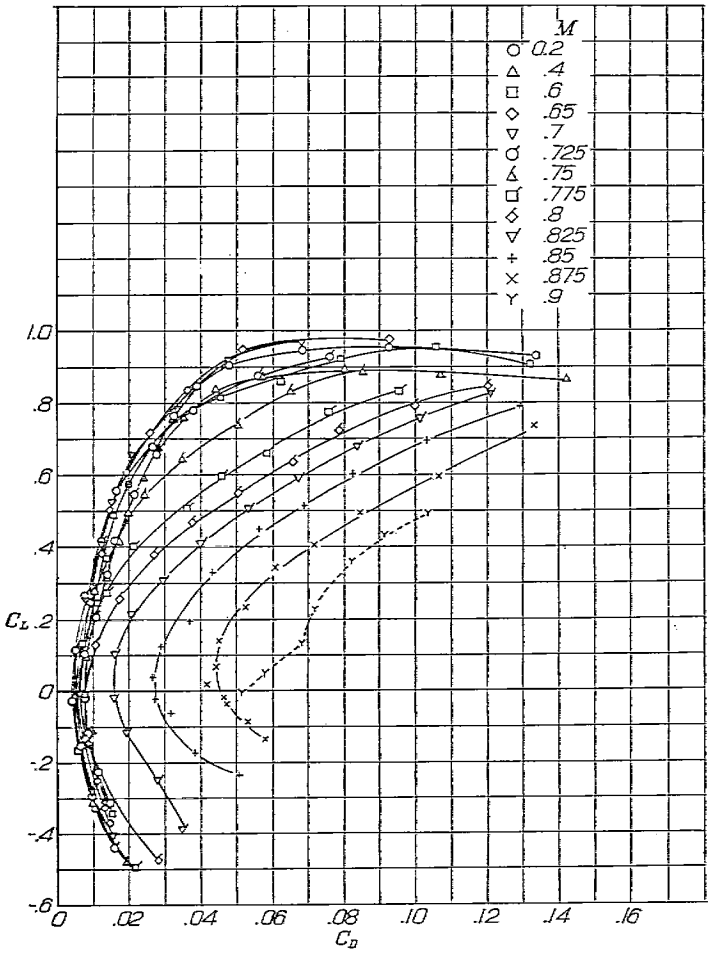

FIGURE 21.—Variation of drag coefficient with lift coefficient for the NACA 65$_1$-212 wing of aspect ratio 10.8.

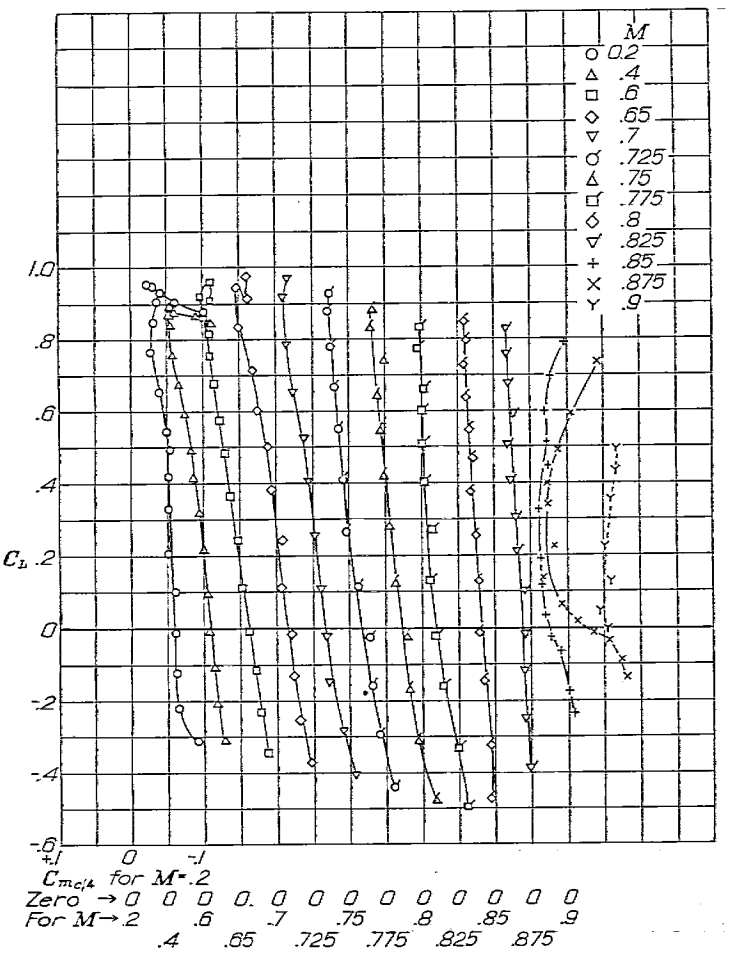

FIGURE 22.—Variation of pitching-moment coefficient with lift coefficient for the NACA 65$_1$-212 wing of aspect ratio 10.8.

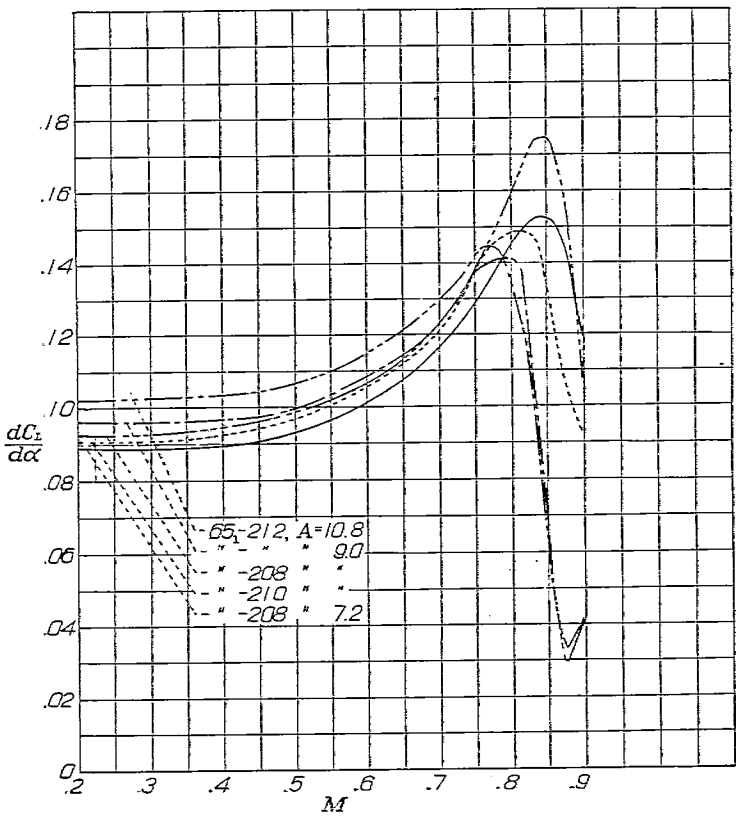

FIGURE 23.—Lift-curve slopes for five wings having NACA 65$_1$-series airfoil sections.

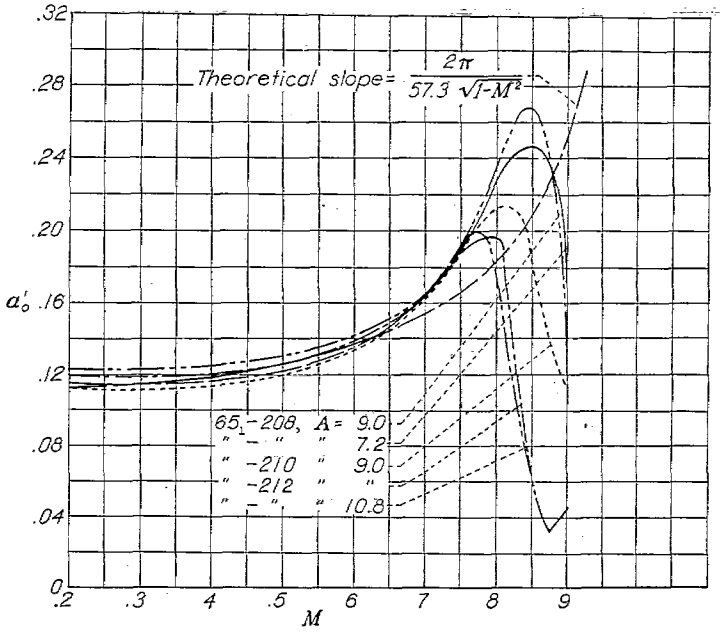

FIGURE 24.—The variation, with Mach number, of the estimated section lift-curve slopes for five wings having NACA 65₁-series airfoil sections.

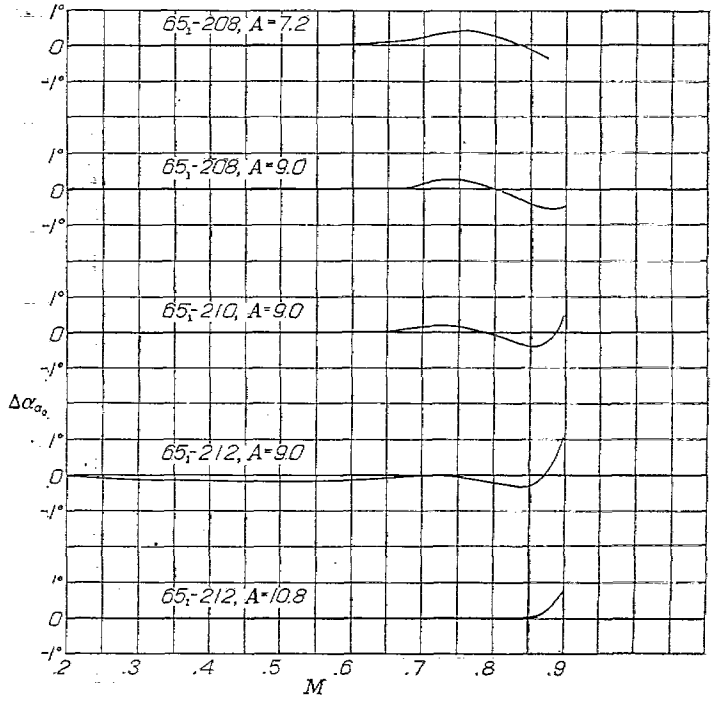

FIGURE 25.—Changes in angle of attack for zero lift from the low-speed value for five wings having NACA 65₁-series airfoil sections.

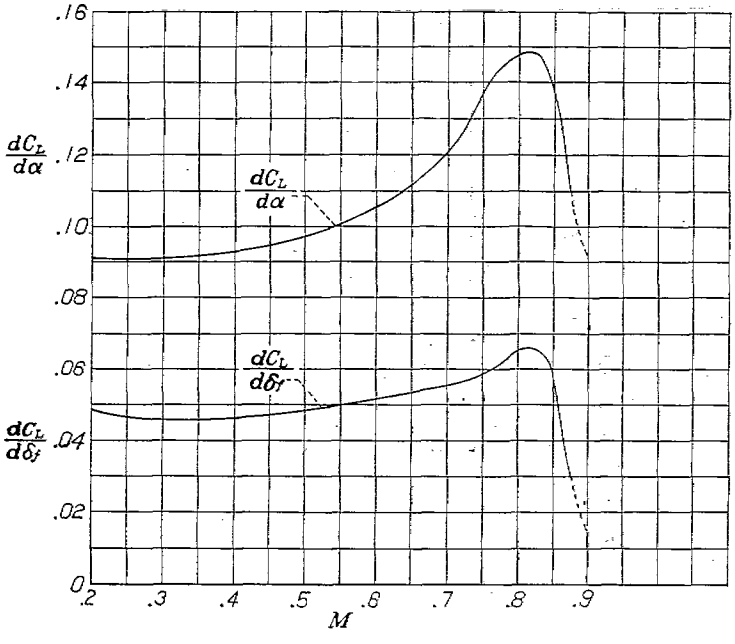

FIGURE 26.—Variation of the lift-curve slope and flap effectiveness with Mach number for the NACA 65₁-210 wing of aspect ratio 9 with a 0.20 chord flap.

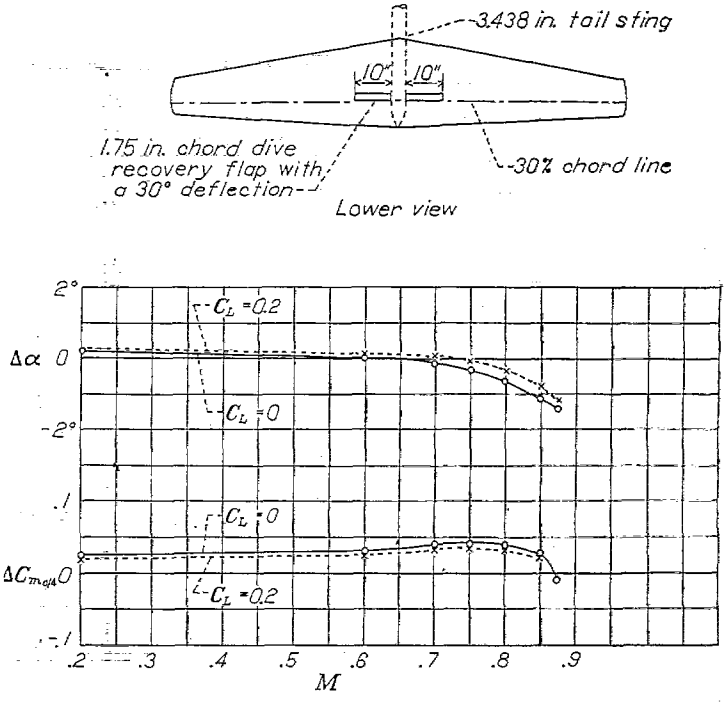

FIGURE 27.—Increments of angle of attack and pitching-moment coefficient due to the deflection of a dive-recovery flap on the NACA 65₁-208 wing of aspect ratio 7.2.

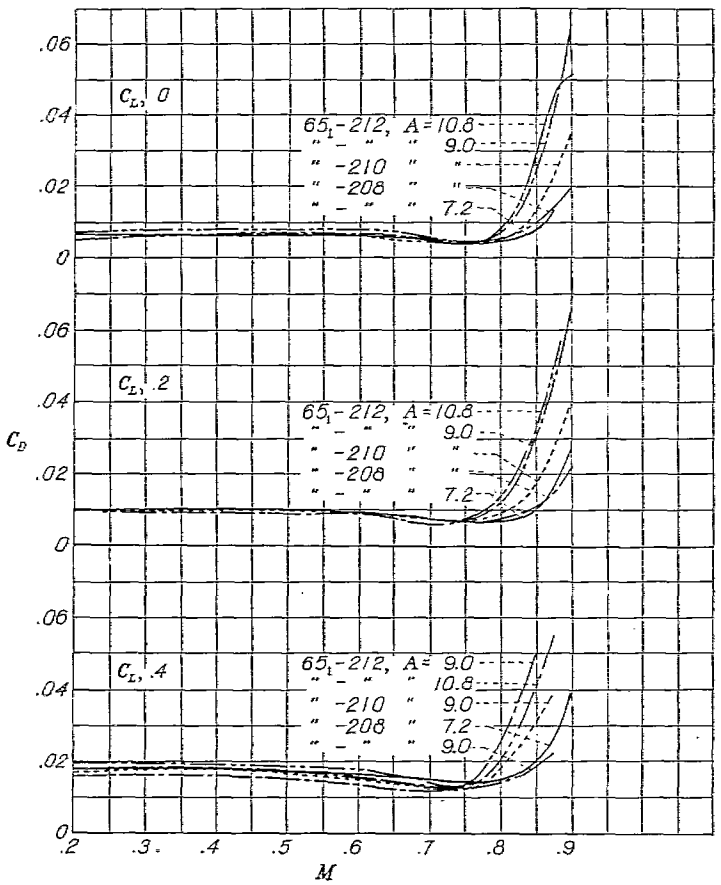

FIGURE 28.—Drag coefficients for five wings having NACA 65$_1$-series airfoil sections.

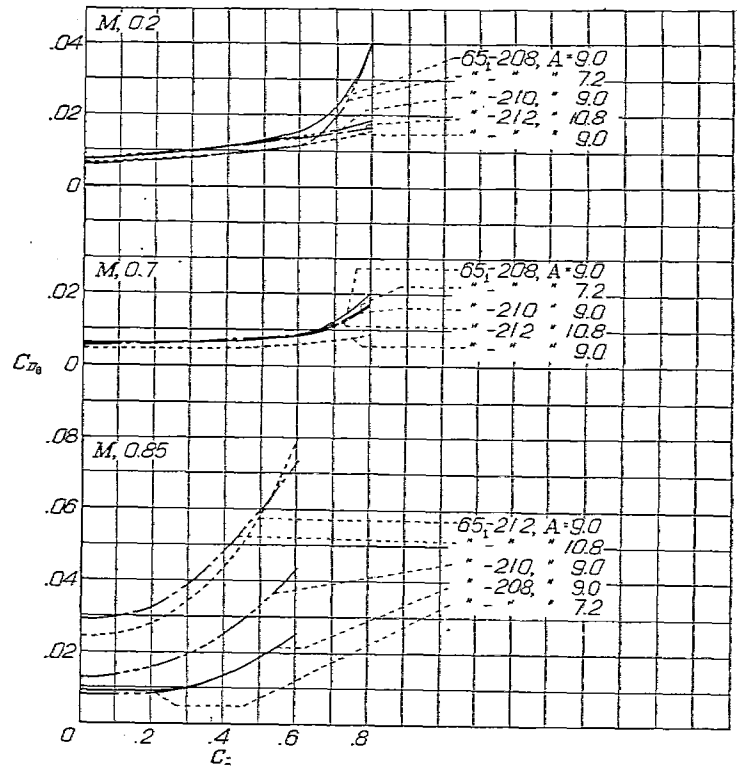

FIGURE 29.—Profile drag coefficients for five wings having NACA 65$_1$-series airfoil sections

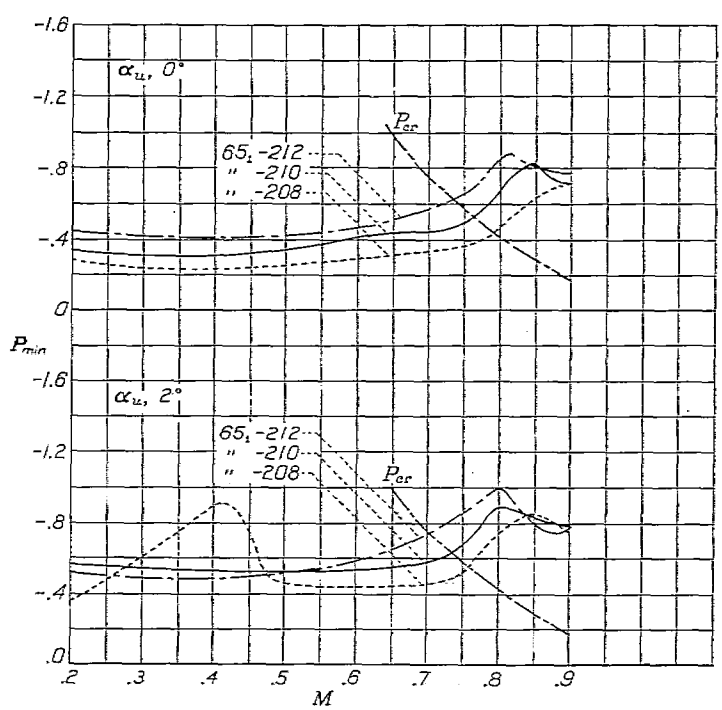

FIGURE 30.—Variation of upper-surface minimum-pressure coefficients with Mach number for wing station 10.0 on three NACA 65$_1$-series wings of aspect ratio 9 with the fuselage.

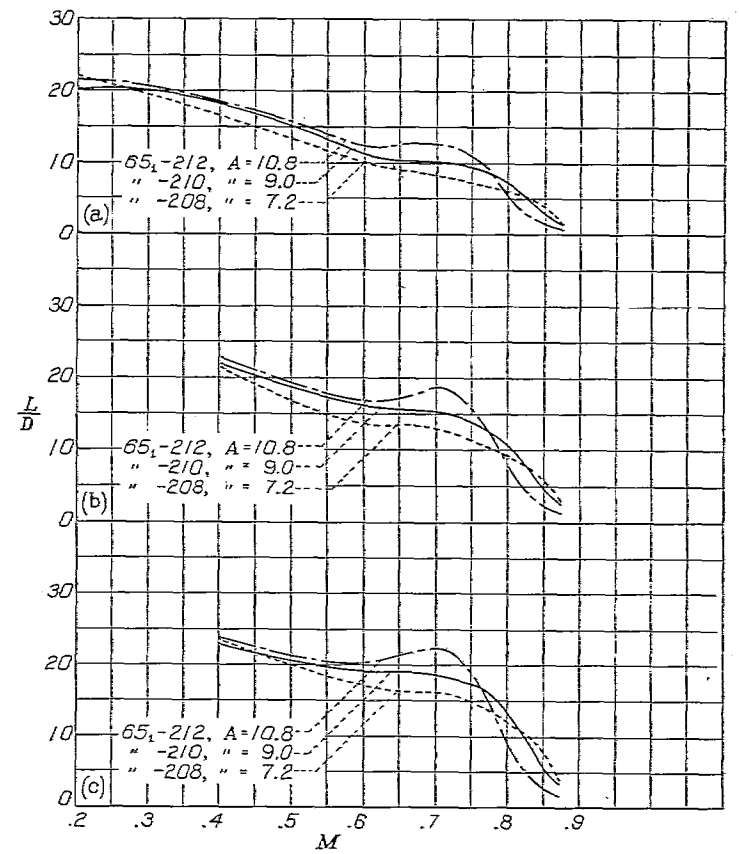

(a) Weight corresponding to a wing loading of 40 pounds per square foot for the wing of aspect ratio 9.

(b) Weight corresponding to a wing loading of 60 pounds per square foot for the wing of aspect ratio 9.

(c) Weight corresponding to a wing loading of 80 pounds per square foot for the wing of aspect ratio 9.

FIGURE 31.—A comparison for a level-flight condition at sea level of the lift-drag ratios for three NACA 65$_1$-series wings having the same absolute thickness and span but different chords.

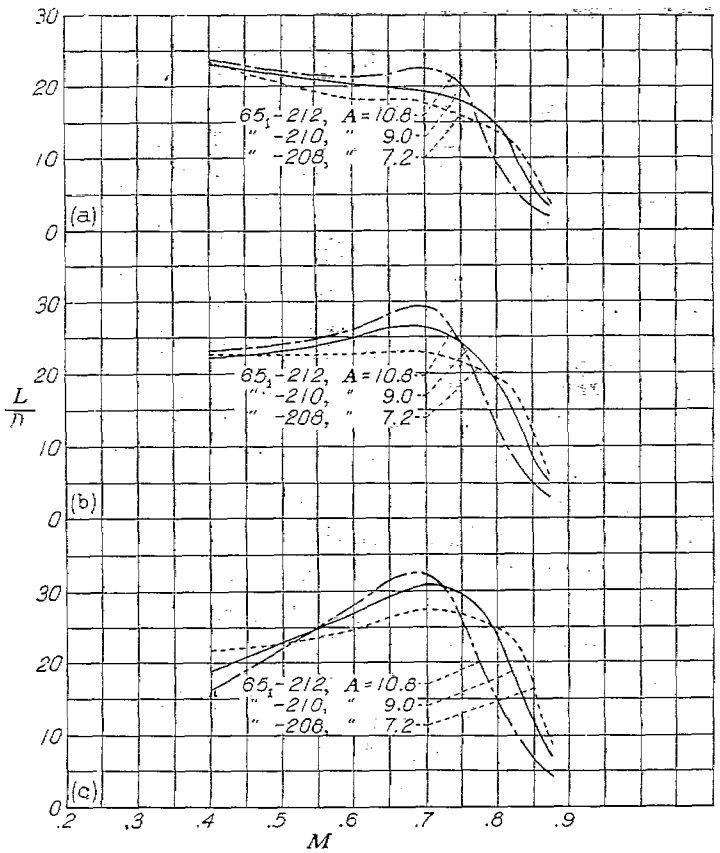

(a) Weight corresponding to a wing loading of 40 pounds per square foot for the wing of aspect ratio 9.

(b) Weight corresponding to a wing loading of 60 pounds per square foot for the wing of aspect ratio 9.

(c) Weight corresponding to a wing loading of 80 pounds per square foot for the wing of aspect ratio 9.

FIGURE 32.—A comparison for a level-flight condition at 20,000 feet altitude of the lift-drag ratios for three NACA 65_1-series wings having the same absolute thickness and span but different chords.

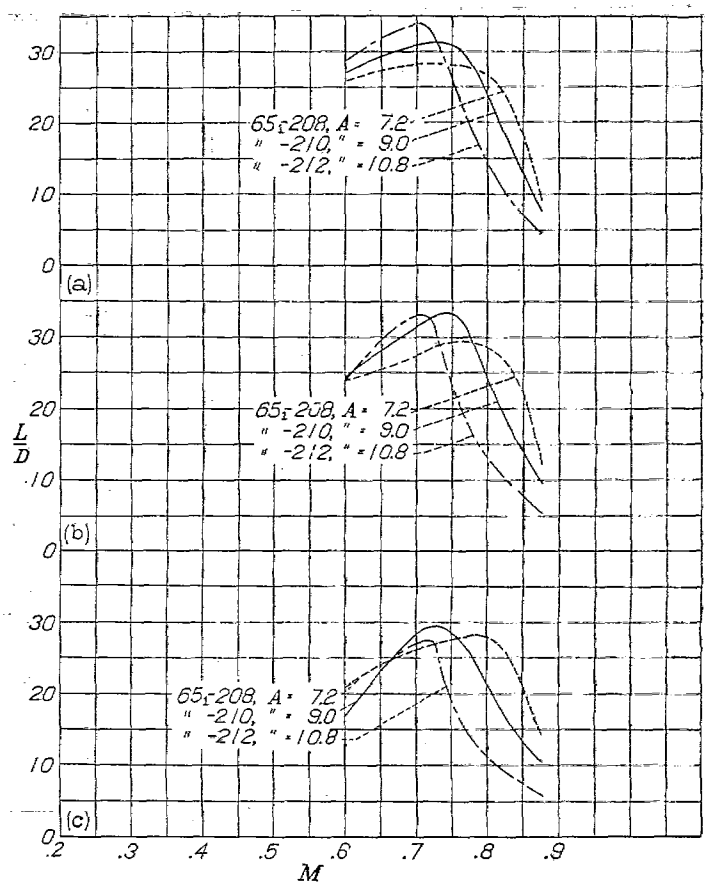

(a) Weight corresponding to a wing loading of 40 pounds per square foot for the wing of aspect ratio 9.

(b) Weight corresponding to a wing loading of 60 pounds per square foot for the wing of aspect ratio 9.

(c) Weight corresponding to a wing loading of 80 pounds per square foot for the wing of aspect ratio 9.

FIGURE 33.—A comparison for a level-flight condition at 40,000 feet altitude of the lift-drag ratios for three NACA 65_1-series wings having the same absolute thickness and span but different chords.

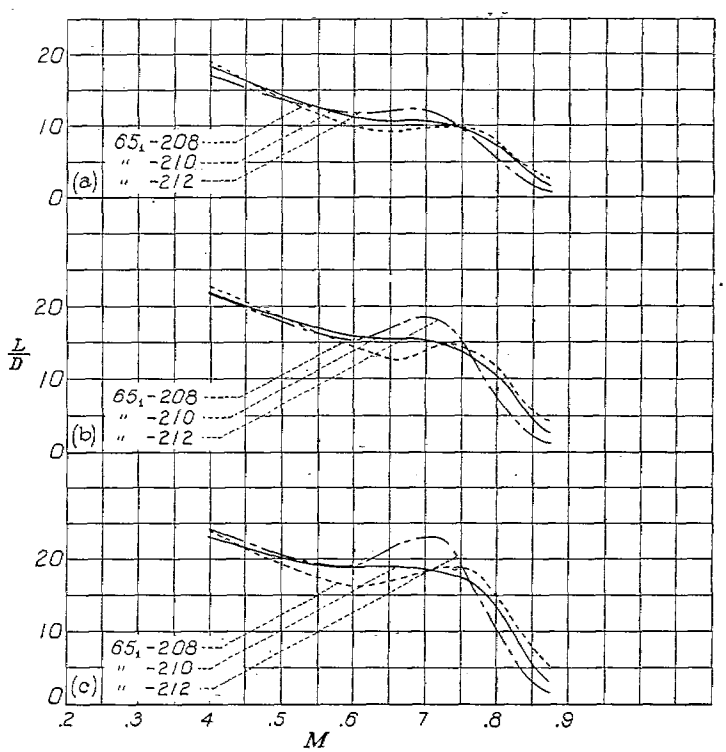

(a) Wing loading, 40 pounds per square foot. (b) Wing loading, 60 pounds per square foot. (c) Wing loading, 80 pounds per square foot.

FIGURE 34.—A comparison for a level-flight condition at sea level of the lift-drag ratios for three NACA 65_1-series wings of aspect ratio 9.

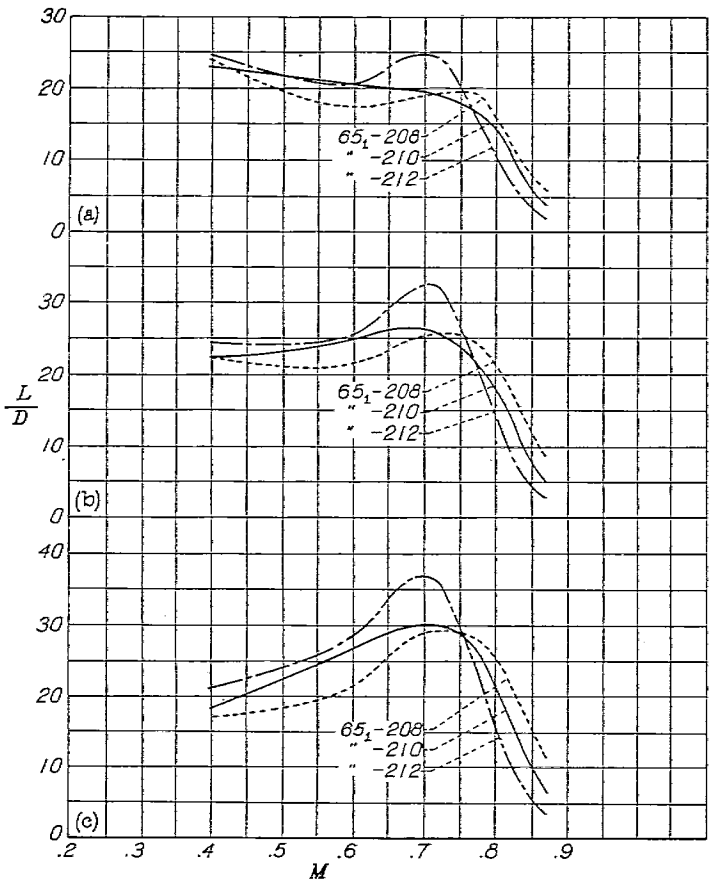

(a) Wing loading, 40 pounds per square foot.
(b) Wing loading, 60 pounds per square foot.
(c) Wing loading, 80 pounds per square foot.

FIGURE 35.—A comparison for a level-flight condition at 20,000 feet altitude of the draglift. ratios for three NACA 65$_1$-series wings of aspect ratio 9.

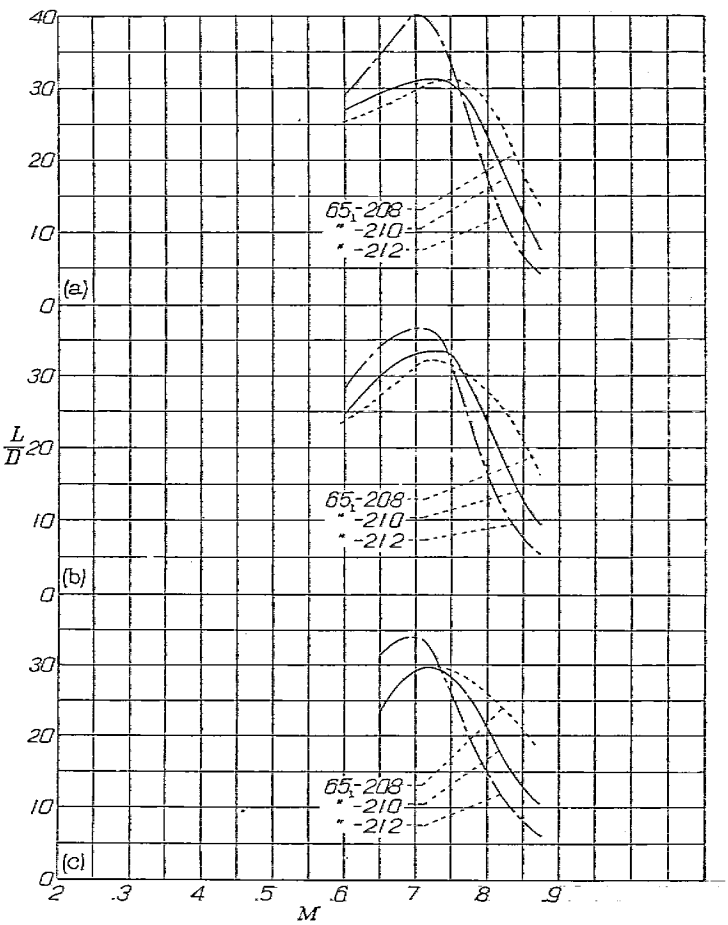

(a) Wing loading, 40 pounds per square foot.
(b) Wing loading, 60 pounds per square foot.
(c) Wing loading, 80 pounds per square foot.

FIGURE 36.—A comparison for a level-flight condition at 40,000 feet altitude of the lift-drag ratios for three NACA 65$_1$-series wings of aspect ratio 9.

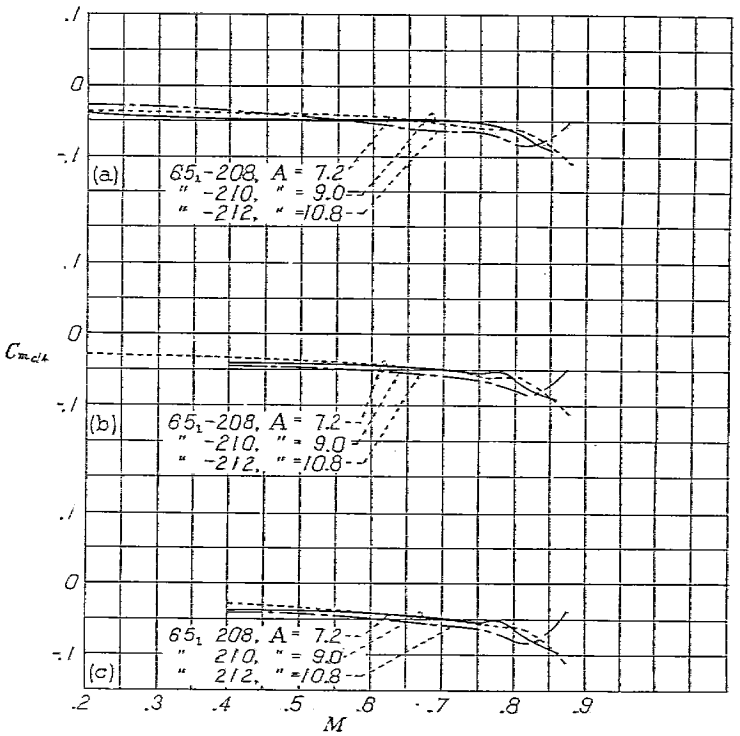

(a) Weight corresponding to a wing loading of 40 pounds per square foot for the wing of aspect ratio 9.
(b) Weight corresponding to a wing loading of 60 pounds per square foot for the wing of aspect ratio 9.
(c) Weight corresponding to a wing loading of 80 pounds per square foot for the wing of aspect ratio 9.

FIGURE 37.—A comparison for a level-flight condition at sea level of the pitching-moment coefficients for three NACA 65$_1$-series wings having the same absolute thickness and span but different chords.

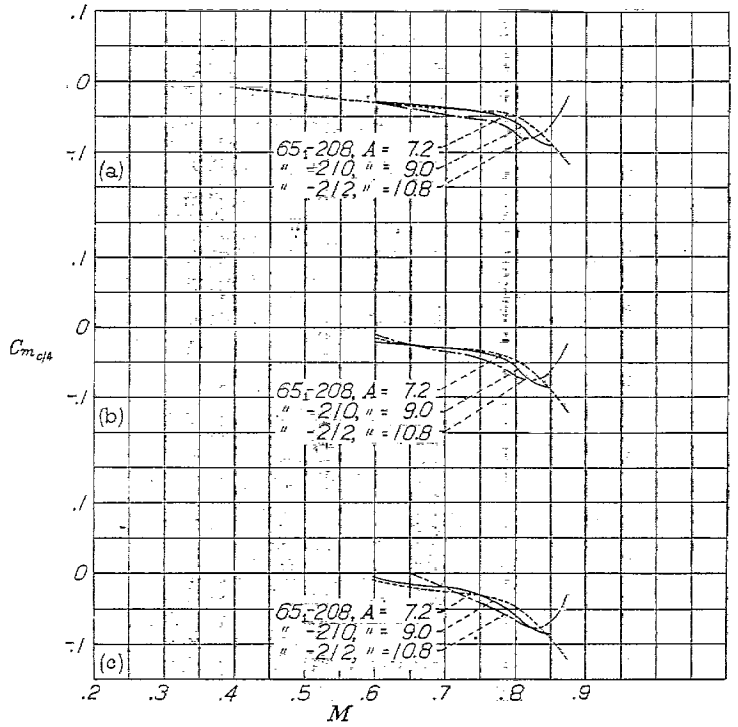

(a) Weight corresponding to a wing loading of 40 pounds per square foot for the wing of aspect ratio 9.

(b) Weight corresponding to a wing loading of 60 pounds per square foot for the wing of aspect ratio 9.

(c) Weight corresponding to a wing loading of 80 pounds per square foot for the wing of aspect ratio 9.

FIGURE 38.—A comparison for a level-flight condition at 40,000 feet altitude of the pitching-moment coefficients for three NACA 65_1-series wings having the same absolute thickness and span but different chords.

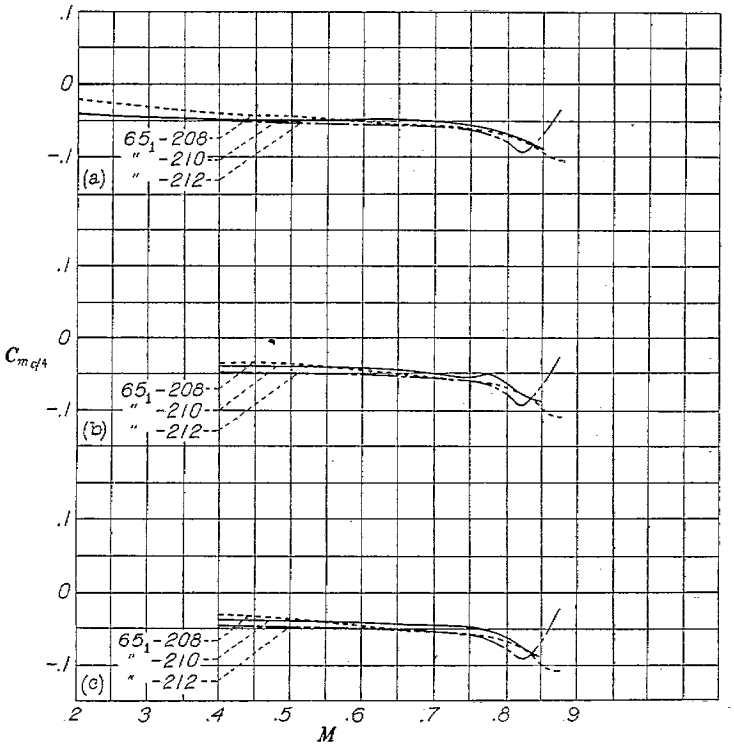

(a) Wing loading, 40 pounds per square foot.
(b) Wing loading, 60 pounds per square foot.
(c) Wing loading, 80 pounds per square foot.

FIGURE 39.—A comparison for a level-flight condition at sea level of the pitching-moment coefficients for three NACA 65_1-series wings of aspect ratio 9.

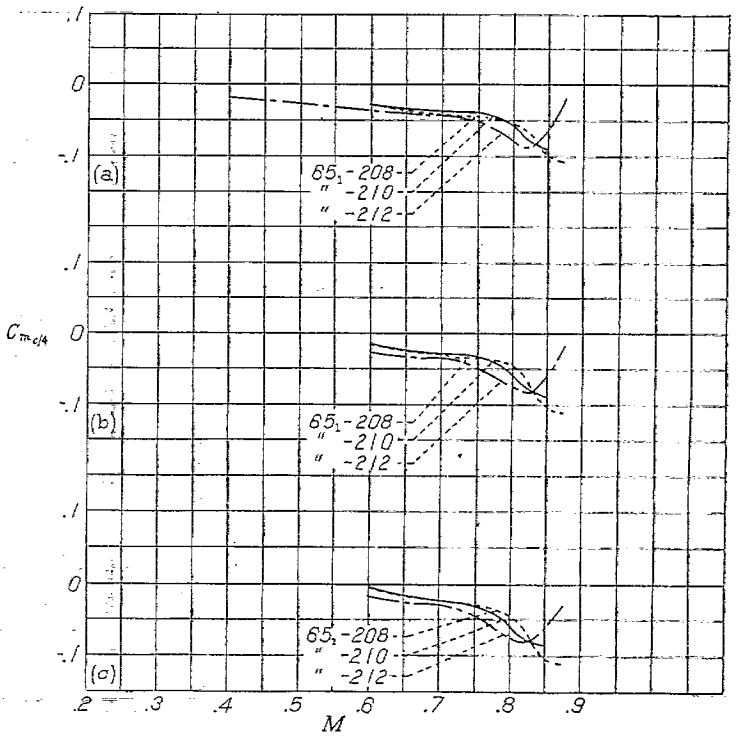

(a) Wing loading, 40 pounds per square foot.
(b) Wing loading, 60 pounds per square foot.
(c) Wing loading, 80 pounds per square foot.

FIGURE 40.—A comparison for a level-flight condition at 40,000 feet altitude of the pitching-moment coefficients for three NACA 65_1-series wings of aspect ratio 9.

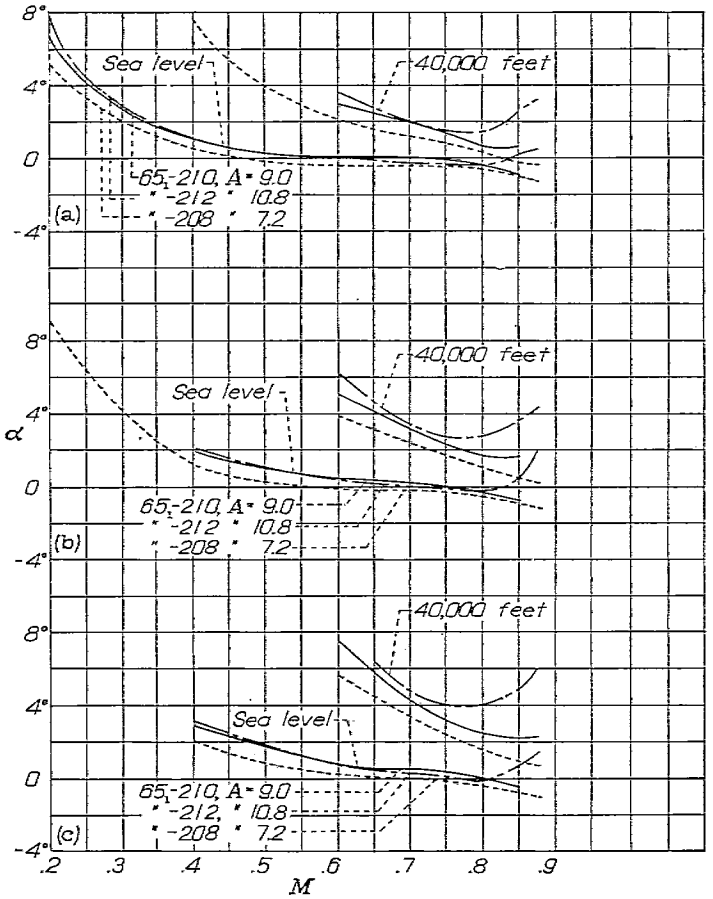

(a) Weight corresponding to a wing loading of 40 pounds per square foot for the wing of aspect ratio 9.
(b) Weight corresponding to a wing loading of 60 pounds per square foot for the wing of aspect ratio 9.
(c) Weight corresponding to a wing loading of 80 pounds per square foot for the wing of aspect ratio 9.

FIGURE 41.—Angle of attack required for level flight for three NACA 65_1-series wings having the same absolute thickness and span but different chords.

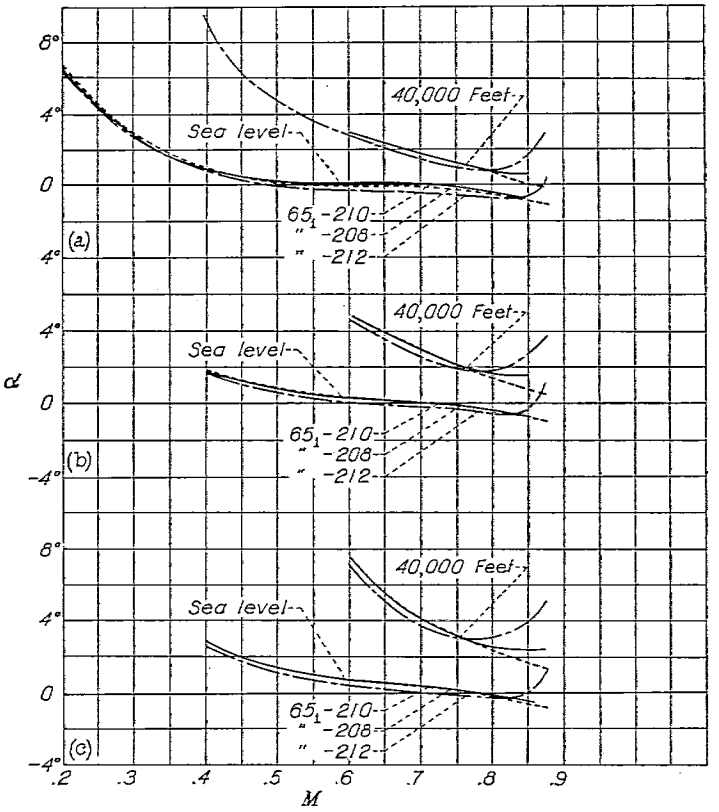

(a) Wing loading, 40 pounds per square foot.
(b) Wing loading, 60 pounds per square foot.
(c) Wing loading, 80 pounds per square foot.

FIGURE 42.—Angle of attack required for level flight for three NACA 65_1-series wings of aspect ratio 9.